HHS Public Access

Author manuscript

Physiol Behav. Author manuscript; available in PMC 2022 January 01.

Published in final edited form as:

Physiol Behav. 2021 January 01; 228: 113183. doi:10.1016/j.physbeh.2020.113183.

Nociceptin/orphanin FQ neurons in the Arcuate Nucleus and Ventral Tegmental Area Act via Nociceptin Opioid Peptide Receptor Signaling to Inhibit Proopiomelanocortin and A_{10} Dopamine Neurons and Thereby Modulate Ingestion of Palatable Food

Jennifer Hernandez[2], **Lynnea Perez**[1], **Rosy Soto**[2], **Nikki Le**[1], **Cassandra Gastelum**[1], **Edward J. Wagner**[1,2,#]

[1]Graduate College of Biomedical Sciences, Western University of Health Sciences, Pomona, CA, USA

[2]College of Osteopathic Medicine of the Pacific, Western University of Health Sciences, Pomona, CA, USA

Abstract

The neuropeptide nociceptin/orphanin FQ (N/OFQ) inhibits neuronal activity via its cognate nociceptin opioid peptide (NOP) receptor throughout the peripheral and central nervous systems, including those areas involved in the homeostatic and hedonic regulation of energy homeostasis. We thus tested the hypothesis that N/OFQ neurons in the hypothalamic arcuate nucleus (ARC) and ventral tegmental area (VTA) act via NOP receptor signaling to inhibit nearby anorexigenic proopiomelanocortin (POMC) and A_{10} dopamine neuronal excitability, respectively, and thereby modulate ingestion of palatable food. Electrophysiologic recordings were performed in slices prepared from transgenic male and ovariectomized (OVX) female N/OFQ-cre/enhanced green fluorescent protein-POMC, N/OFQ-cre and tyrosine hydroxylase-cre animals to see if optogenetically-stimulated peptide release from N/OFQ neurons could directly inhibit these neuronal populations. Binge-feeding behavioral experiments were also conducted where animals were exposed to a high-fat-diet (HFD) for one hour each day for five days and monitored for

[#]Corresponding Author: Edward J. Wagner, College of Osteopathic Medicine of the Pacific, Western University of Health Sciences, 309 E. 2nd Street, Pomona, CA 91766, USA, Tel: 1-909-469-5239, ewagner@westernu.edu.

Author Contributions

JH, LP, CG and NL performed all stereotaxic and survival surgeries. JH and LP performed all electrophysiological recordings. JH, LP, CG, RS, and NL performed all metabolic studies. JH, LP and EJW performed data analysis for all electrophysiology and metabolic studies. JH, LP, and EJW created all figures and performed all statistical analyses. EJW generated the manuscript, while all authors edited the final manuscript. EJW, JH, and LP designed the experiments.

Statement of Ethics

All procedures were approved by the Western University of Health Sciences' IACUC in accordance with institutional guidelines based on NIH standards.

Disclosure Statement

The authors have no conflicts of interest to declare.

energy intake. Photostimulation of ARC and VTA N/OFQ neurons produces an outward current in POMC and A_{10} dopamine neurons receiving input from these cells. This is associated with a hyperpolarization and decreased firing. These features are also sex hormone- and diet-dependent; with estradiol-treated slices from OVX females being less sensitive, and obese males being more sensitive, to N/OFQ. Limited access to HFD causes a dramatic escalation in consumption, such that animals eat 25–45% of their daily intake during that one-hour exposure. Moreover, the NOP receptor-mediated regulation of these energy balance circuits are engaged, as N/OFQ injected directly into the VTA or ARC respectively diminishes or potentiates this binge-like increase in a manner heightened by diet-induced obesity or dampened by estradiol in females. Collectively, these findings provide key support for the idea that N/OFQ regulates appetitive behavior in sex-, site- and diet-specific ways, along with important insights into aberrant patterns of feeding behavior pertinent to the pathogenesis of food addiction.

Graphical Abstract

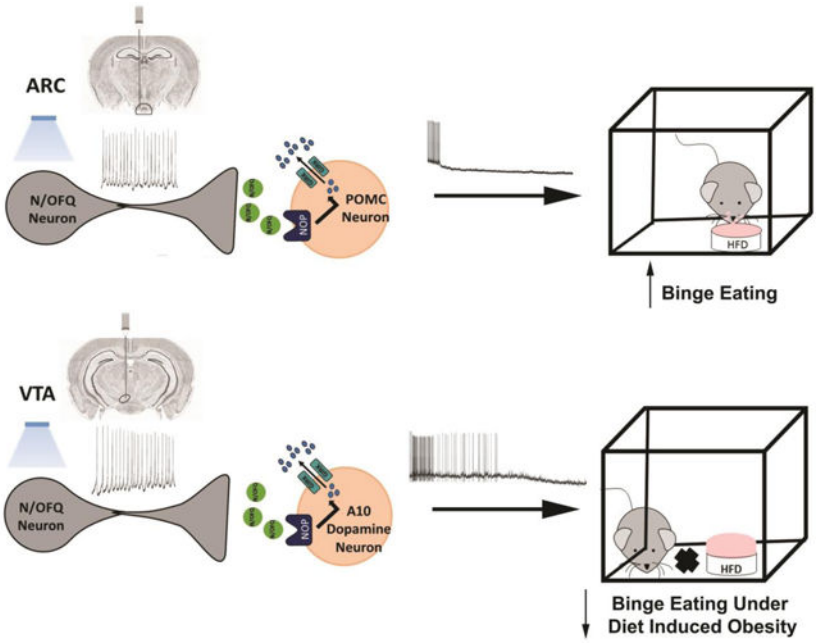

Keywords

Nociceptin; POMC; A_{10} dopamine neurons; VTA; ARC; energy balance; food addiction; sex differences

1. INTRODUCTION

Energy homeostasis, the intricate balance between energy intake and expenditure, is regulated in coordinate fashion by homeostatic and hedonic neural circuits [1, 2]. Aberrations in these circuits are implicated in the pathophysiology of conditions such as obesity, type-II diabetes, and food addiction [3–5]. Homeostatic control is attributed to the

hypothalamic energy balance circuitry, relaying anorexigenic and orexigenic signals to stimulate or suppress energy intake.

Excitatory input from steroidogenic factor 1 (SF-1) neurons, located in the hypothalamic ventromedial nucleus (VMN), impinging on proopiomelanocortin (POMC) neurons in the arcuate nucleus (ARC) represent a critical anorexigenic synapse in homeostatic energy balance that, when activated, suppresses energy intake and enhances energy expenditure [5–7]. On the other hand, mechanisms of hedonic energy balance regulation involve the mesolimbic dopamine (A_{10}) neurons that originate in the ventral tegmental area (VTA) and project to the nucleus accumbens and prefrontal cortex [8–10]. A_{10} dopamine neurons encode reward processing for natural and drug-induced rewards and are implicated in increasing incentive salience for palatable foods, food-seeking behavior and impulsivity that could, under the right circumstances, lead to binge-feeding behavior [4, 8, 10–13]. Indeed, dopamine release into the nucleus accumbens and c-fos expression in A_{10} dopamine neurons is increased during binge-feeding episodes [14, 15]; lending further credence to this notion.

The neuropeptide nociceptin/Orphanin FQ (N/OFQ), and its cognate $G_{i/o}$-coupled nociceptin opioid receptor (NOP), are densely expressed in the ARC and VTA [16–18], supporting a role in both homeostatic and hedonic energy balance regulation. Exogenously administered N/OFQ inhibits anorexigenic ARC POMC neurons pleiotropically, in part by activation of G-protein coupled inwardly-rectifying K+ (GIRK) channels, in a sex- and diet-dependent manner [5, 19]. Males respond more robustly to the inhibitory effects of exogenous N/OFQ on excitatory neurotransmission at VMN SF-1/ARC POMC synapses than do females at estradiol-dominated phases of the estrous cycle [5]. In addition, diet-induced obesity renders ARC N/OFQ neurons hyperexcitable, and increases the sensitivity of VMN SF-1/ARC POMC synapses to the inhibitory effects of exogenous N/OFQ in males and ovariectomized (OVX) females [5, 20]. Moreover, estradiol attenuates the inhibitory effects of exogenous N/OFQ at VMN SF-1/ARC POMC synapses, and protects against the deranged hyperphagia and reduction in energy expenditure caused by exogenous N/OFQ administered directly into the ARC of obese OVX females [5, 19, 21]. Furthermore, N/OFQ suppresses A_{10} dopamine neuronal excitability and dopamine release [22–24]. However, the exact mechanisms by which sex and diet converge on N/OFQ-mediated inhibition of A_{10} dopamine neurotransmission, and the corresponding effects on the hedonic regulation of energy balance, are still unclear. Therefore, we sought to further elucidate and compare the role of N/OFQ in hedonic and homeostatic regulation of energy balance, assessing actions of endogenous and exogenously administered N/OFQ, and the role of sex and diet in both. We hypothesize that N/OFQ, via NOP receptor signaling, will inhibit VTA A_{10} dopamine and ARC POMC neuronal excitability to disparately influence hedonic and homeostatic energy balance.

2. MATERIALS AND METHODS

2.1. Animal Models

Tyrosine hydroxylase (TH)-cre mice generated on a C57BL/6 background were purchased from Jackson Laboratories (Stock # 008601; Bar Harbor, ME, USA), and bred in-house. N/OFQ-cre (aka PNOC-cre [25]) mice (C57BL/6 background) were obtained from Dr. Michael

Brucas at the University of Washington and also bred in-house. For some experiments, N/OFQ-cre/(enhanced green fluorescent protein (eGFP) POMC mice were generated in-house by breeding hemizygous N/OFQ-cre mice with hemizygous eGFP-POMC mice (Jackson Laboratories; Stock #009593; C57BL/6 background). All animals are provided food and water ad libitum, maintained under constant temperature (25°C) and kept on a 12hour light – 12hour dark schedule (lights on 06:00–18:00). Genetic karyotyping for each animal was accomplished using established PCR procedures. At weaning, animals were randomly assigned to one of two dietary groups. Some animals received a standard chow diet (Teklad Rodent Diet, Teklad Diets, Madison, WI, USA) from which 18% of the calories are derived from fat, 24% from protein, and 58% from carbohydrates. Others were exposed to a high-fat diet (HFD; Research Diets, New Brunswick, NJ, USA) – from which 45% of calories were derived from fat, 20% from protein and 35% from carbohydrates – for 5–8 weeks prior to experimentation. We have demonstrated previously that the consumption of this HFD over this period of time produces overt adiposity and glucose intolerance [5, 26, 27]. All studies described below will be performed in accordance with the NIH Guide for the Care and Use of Laboratory Animals, and approved by our institutional animal care and use committee.

2.2. Surgical Procedures

For all experiments, female N/OFQ-cre, TH-cre, N/OFQ-cre/eGFP POMC and wildtype mice were ovariectomized (OVX) while they were under 2% isoflurane anesthesia five days before experimentation. In order to focally inject adeno-associated viral vector (AAV) constructs, OFQ-Cre, TH-Cre, and N/OFQ-cre/eGFP POMC mice were anesthetized with 2% isoflurane and placed on a stereotaxic frame (Stoelting, Wood Dale, IL, USA). An incision was made to expose the skull, and a hole was drilled on one or both sides of the mid-sagittal suture so that an injection needle could be slowly lowered into the ARC (coordinates from bregma: AP, −0.6mm; ML, ± 0.3mm; and DV, −5.9mm from dura) for N/OFQ-cre/eGFP POMC mice and the VTA (coordinates from bregma: AP, −2.1mm; ML, ± 0.5mm; and DV, −4.2mm from dura) for N/OFQ-Cre and TH-Cre mice. Unilateral injections of a cre recombinase-dependent AAV vector respectively containing either cation channel rhodopsin-2 (ChR2 [28]; AAV1.EF1a.DIO.ChR2 (E123A).YFP.WPRE.jGH; 7.2×10^{12} genomic copies/mL; 300nL total volume; Addgene plasmid #35507) or its enhanced yellow fluorescent protein (eYFP) blank control ([28]; pAAV-Ef1a-DIO EYFP; 1.0×10^{13}; 300 nL total volume; Addgene plasmid #27056) were given over 2 minutes. The injection needle remained in place for 10 minutes after infusion to allow for diffusion from the tip, and then slowly removed from the brain to reduce inadvertent spread of the virus. Animals were used for experimentation 2–3 weeks after viral injection.

The stereotaxic implantation of a guide cannula into the ARC or VTA of wildtype mice was performed similar to that described above. Briefly, once anesthetized, an animal was secured on a stereotaxic frame and a midline incision was made through the scalp. A hole was then drilled in the skull, through which a 26-gauge guide cannula (Plastics One, Roanoke, VA, USA) was lowered 1 mm above the ARC (AP, −0.6mm; ML, ± 0.3mm; and DV, −4.9mm) or the VTA (AP, −2.1mm, ML, ±0.5 mm, DV, −3.2 mm). Guide cannulas were fastened in place with C&B Metabond dental cement (Parkell, Edgewood, NY, USA) applied to the surgical field. Finally, a stylet was inserted into the guide cannula to keep the lumen patent.

The animals were allowed to recover for 1 week prior to the start of experimentation. At the time of injection, an injector needle was inserted such that its tip protruded 1 mm below the tip of the guide cannula shaft and into the region of interest. We have extensive experience in stereotaxically probing deep brain structures [5, 19, 21], and this is amply reflected in the schematic shown in Supplementary Fig. 1. Only those animals whose injection sites or guide cannulas were accurately placed within the VTA or ARC were used in the present study.

2.3. Drugs

All drugs were purchased from Tocris Bioscience/R&D Systems (Minneapolis, MN, USA) unless otherwise stated. For electrophysiological experiments, the Na^+ channel blocker octahydro-12-(hydroxymethyl)-2-imino-5,9:7,10a-dimethano-10aH-[1,3]dioxocino[6,5-d]pyrimidine-4,7,10,11,12-pentol (Tetrodotoxin, TTX) was prepared as a 1mM stock solution in UltraPure H_20, and diluted further with aCSF to the working concentration of 500nM. N/OFQ was prepared as a 1mM stock solution in UltraPure H_20, and diluted further with aCSF to the working concentration of 1μM. The NOP receptor antagonist (2R)-1-(Phenylmethyl)-N-[3-(spiro[isobenzofuran-1(3H),4'-piperidin]-1-yl)propyl-2-pyrrolidinecarboxamide (BAN ORL 24) was prepared as a 10mM stock solution in UltraPure H_2O, and diluted further with aCSF to the working concentration of 10μM. 1, 3, 5(10)-Estratrien-3, 17β-diol (17β-estradiol; E_2; Steraloids, RI, USA) was dissolved in punctilious ethanol to a stock concentration of 1mM, which was further diluted to a working concentration of 100nM.

For all behavioral experiments, N/OFQ was prepared as a 1.5mM stock solution by dissolving it in filtered saline, and injected directly into the ARC or VTA at a 0.3nmol dose. Estradiol benzoate (EB; Steraloids, Newport, RI, USA) was used in lieu of E_2 in this context because it is a prodrug requiring biotransformation and therefore prolongs the half-life of E_2. It was initially prepared as a 1 mg/mL stock solution in punctilious ethanol. A known quantity of this stock solution was added to a volume of sesame oil sufficient to produce a final concentration of 20 μg/mL following evaporation of the ethanol. [$Nphe^1$,Arg^{14},Lys^{15}]Nociceptin-NH_2 (UFP-101) was prepared as a 14mM stock solution by dissolving it in filtered saline, and injected directly into the VTA at a 10nmol dose along with N/OFQ. All aliquots of the stock solutions were stored at either four or −20 °C until needed for experimentation.

2.4. Brain Slice Preparation

On the day of experimentation, the animal was briefly anesthetized with 32% isoflurane and rapidly decapitated. The brain was removed from the skull and dissected to procure hypothalamic or mesencephalic slices in the coronal plane. The resultant block was then mounted on a cutting platform that was secured in a vibratome well filled with an ice-cold, oxygenated (95% O_2, 5%CO_2) sucrose-based cutting solution (NaHCO3 26; dextrose 10, HEPES 10; Sucrose 208; KCl 2; NaH_2PO_4 1.25; $MgSO_4$ 2; $CaCl_2$ 1; in mM). In this manner, we were able to obtain four to five slices (300μm) through the rostrocaudal extent of the ARC, and two to three slices (250μm) through the rostrocaudal extent of the VTA. The slices were transferred to an auxiliary chamber containing oxygenated aCSF at room temperature, and maintained there until the electrophysiological recording.

2.5. Electrophysiology

Whole-cell patch clamp electrophysiological recordings from ARC and VTA neurons using biocytin-filled electrodes were performed in hypothalamic and mesencephalic slices prepared from intact male and OVX female TH-cre, N/OFQ-cre and N/OFQ-cre/eGFP-POMC mice. During recordings, the slices were maintained in a chamber perfused with warmed (35 °C), oxygenated aCSF in which the $CaCl_2$ concentration raised to 2mM. Artificial CSF and all drugs (diluted with aCSF) were perfused via peristaltic pump at a rate of 1.5 mL/min. Patch electrodes were prepared from borosilicate glass (World Precision Instruments, Sarasota, FL, USA; 1.5 mm OD) pulled on a P-97 Flaming Brown puller (Sutter Instrument Co., Novato, CA, USA), and filled with an internal solution containing the following (in mM): potassium gluconate 128; NaCl 10; $MgCl_2$ 1; EGTA 11; HEPES 10; ATP 1; GTP 0.25; 0.5% biocytin; adjusted to a pH of 7.3 with KOH; osmolality: 286–320 mOsm. Electrode resistances varied from 3 to 8 MΩ.

Recordings were made on an Olympus BX51 W1 fixed stage microscope outfitted with infrared differential interference contrast (DIC) video imaging. A Multiclamp 700B preamplifier (Molecular Devices) amplified potentials and passed current through the electrode. Membrane currents and voltages underwent analog-digital conversion with a Digidata 1550A interface (Molecular Devices) coupled to pClamp 10.5 software. The access resistance, resting membrane potential (RMP), and input resistance were monitored throughout the course of all recordings. If the access resistance deviated greater than 10% of the original value, the recording was ended. Low-pass filtering of the currents was conducted at a frequency of 2 kHz. The liquid junction potential was calculated to be −10mV, and corrected for during data analysis using pClamp software. All recordings were performed at a holding potential of −60mV.

To determine the postsynaptic effects elicited by bath application of N/OFQ, we first performed recordings in slices from TH-cre mice injected 2–3 weeks prior with a eYFP blank-containing AAV into the VTA. We initially generated a baseline current-voltage (I/V) relationship from a holding potential of −60 mV by administering pulses (10-mV increments; 150 msec duration) ranging from −50 to −130 mV. For voltage clamp experiments, baseline I/V relationships were generated in the presence of 500 nM TTX. After the baseline I/V, N/OFQ (1 μM) was added along with TTX, and the membrane current continuously monitored until a new steady-state value was reached, at which time a second I/V relationship was generated. During the N/OFQ washout, the membrane current was again monitored until it returned to its original baseline level, at which time a final I/V relationship is taken to ensure reversibility of the N/OFQ-induced effect. For current clamp experiments, the membrane potential and firing rate were monitored from rest in the absence of TTX until new, N/OFQ-induced steady-state levels were achieved, and then monitored for an additional 10–20 minutes to allow for the return to baseline. To determine if these postsynaptic effects are NOP receptor-mediated and negatively modulated by estradiol, these same recordings were performed in slices pre-treated with 10μM BAN ORL 24 or 100 nM E_2, respectively. Lastly, to ascertain whether diet-induced obesity enhances the sensitivity of A_{10} dopamine neurons to the inhibitory effect of N/OFQ, some recordings were performed in mesencephalic slices prepared from male TH-cre mice fed a HFD for at least five weeks.

For the optogenetic experiments, recordings were performed in slices from N/OFQ-cre/eGFP-POMC and N/OFQ-Cre mice that were injected with a ChR2-containing viral vector into the ARC or VTA 2–3 weeks prior to experimentation. In preliminary experiments we optogenetically stimulated ARC and VTA N/OFQ neurons over a range of frequencies (10-ms pulses delivered at 1, 5, 10 or 20 Hz for 10 s [29, 30]) from a light-emitting diode (LED) blue light source (470nm) controlled by a variable 2A driver (ThorLabs, Newton, NJ, USA) that directly delivered the light path through the Olympus 40X water-immersion lens. This resulted in a frequency-dependent increase in the firing of ARC and VTA N/OFQ neurons, the pattern of which was virtually identical for cells in both regions (Supplementary Fig. 2; 2I: one-way ANOVA/LSD, $F = 201.78$, $df = 4$, $p < 0.0001$; 2J: $F = 252.33$, $df = 4$, $p < 0.0001$). For all subsequent experiments, once N/OFQ-expressing fibers (visualized with eYFP) impinging on an ARC POMC or VTA neuron were encountered, functional synaptic connectivity was ascertained by administering optogenetic stimulation at 20 Hz for 10 s [29]). In the voltage clamp experiments, baseline I/V relationships were generated in the presence of TTX (500nM) and, in some cases, 100 nM E_2, or 10μM BAN ORL 24, respectively. After generating baseline IV's, we applied the photo-stimulation described above to generate the slow outward current. Once a new steady-state current was reached, we generated a second I/V, after which the membrane current was allowed to return to its original baseline level, at which time a final I/V relationship was taken to ensure reversibility of the optogenetic stimulation. Current clamp experiments designed to ascertain the effect of photoactivating ARC and VTA N/OFQ neurons on membrane potential and firing rate were conducted as described in the preceding paragraph.

2.6. Immunohistochemistry

Slices from TH-Cre mice as well as N/OFQ-cre/eGFP-POMC mice were processed for immunohistochemistry using phenotypic markers of A_{10} dopamine and N/OFQ neurons, respectively. Slices were initially fixed with 4% paraformaldehyde in Sorenson's phosphate buffer (pH 7.4) overnight. They were then immersed for three days in 20% sucrose dissolved in Sorensen's buffer, which was changed daily, and frozen in Tissue-Tek embedding medium (Miles, Inc., Elk-hart, IN, USA) the next day. Coronal sections (20μm) through the VTA and ARC were cut on a cryostat and mounted on chilled slides. These sections were then washed with 0.1M sodium phosphate buffer (PBS; pH 7.4), and then processed overnight with either a monoclonal antibody directed against TH (Immunostar, Inc., Hudson, WI, USA; 1:4000 dilution) or a polyclonal antibodies directed against N/OFQ (Abcam, Cambridge, MA, USA; 1:500 dilution) or the vesicular GABA transporter (VGAT; Life Technologies Corporation, Carlsbad, CA, USA; 1:50). This was followed the next day by two 15-minute washes with PBS, and then a two-hour incubation with either biotinylated goat anti-rabbit (Jackson ImmunoResearch Laboratories, Inc., West Grove, PA, USA) or goat anti-mouse (Life Technologies, Carlsbad, CA, USA, 1:300 for both) secondary antibodies. After another series of three 15-minute PBS washes, there was a final two-hour overlay with streptavidin-Alexa Flour (AF)546 (Molecular Probes, Inc., Eugene, OR, PA, USA; 1:600), followed by a final series of three 30-minute PBS washes and cover slipping the slides. The slides were evaluated using fluorescence immunohistochemistry on a Zeiss Axioskop 2 Plus microscope (Carl Zeiss, Göttingen, Germany).

2.7. Binge-Feeding Studies

The behavioral experiments were conducted using a four-cage, Comprehensive Lab Animal Monitoring System (Columbus Instruments, Columbus, OH, USA) as previously described and validated [5, 31]. We monitored energy intake, meal pattern and energy expenditure in intact male and OVX female wildtype mice; the latter of whom were injected with either EB (20 μg/kg; s.c.) or its sesame oil vehicle (1 mL/kg; s.c.) every other day over the course of the experiment. First, the animals were allowed to acclimate in the experimental chambers over a three-day period. Every afternoon they were weighed, handled, and returned to their respective chambers. After acclimatization, we initiated a five-day monitoring phase. The binge feeding protocol was executed in accordance with slight modifications of paradigms described previously [32]. Briefly, one cohort of animals was exposed to the HFD from 4–5 pm for five consecutive days following the three days of acclimation, and energy intake, meal pattern and energy expenditure were quantified for that 60-minute period. Standard chow was provided *ad libitum* for the other 23 hours. For the long-term HFD-fed animals, they were reintroduced to the HFD following a one-week hiatus and underwent the very same protocol as the HFD-naive animals. Just prior to the start of the one-hour HFD exposure, animals were injected with N/OFQ (0.3nmol) or its 0.9% saline vehicle (0.2 μL) directly into the VTA. One cohort of animals was co-injected with the NOP receptor antagonist UFP101 (10 nmole; 0.2 μL)) to determine if it can block the modulatory effect of exogenously administered N/OFQ on binge feeding behavior.

2.8. Statistical Analyses

The homogeneity of variance was evaluated using Levene's Test. Comparisons between two groups were made with the Student's t-test. Comparisons made between more than two groups were performed using either the one-way or repeated measures multifactorial analysis of variance (ANOVA; with rank transformation where appropriate) followed by the Least Significant Difference (LSD) test, or alternatively via the Kruskal-Wallis test followed by the median-notched box-and-whisker analysis. Differences were considered statistically significant if the alpha probability was 0.05 or less.

3. RESULTS AND FIGURES

3.1 Experiment 1: In Vitro Effects of Endogenous N/OFQ on the Excitability of Anorexigenic POMC Neurons in Male and Female Mice

ARC N/OFQ neurons inhibit POMC neurons via a NOP receptor-mediated mechanism—Previous studies have shown that bath application of N/OFQ inhibits anorexigenic POMC neurons via activation of GIRK channels, an effect that is associated with a membrane hyperpolarization and decrease in firing rate [5, 19, 31]. N/OFQ is appreciably expressed in the ARC [16, 18], and so therefore we tested the hypothesis that ARC N/OFQ neurons would inhibit nearby POMC neurons in a sex-dependent manner. N/OFQ neurons (Fig. 1A & 1C) from male N/OFQ-cre/eGFP-POMC mice injected 2–3 weeks prior with a ChR2/eYFP-containing AAV into the ARC exhibit efficient membrane-delimited expression of the eYFP reporter signal (Fig. 1B–1D), and the fibers emanating from these ARC N/OFQ neurons come into close apposition with neighboring POMC neurons (Fig. 1E–1H). Prominent projections from these ARC N/OFQ neurons can be seen

in the adjacent VMN, where N/OFQ cell bodies are conspicuously absent (Fig. 1I). Voltage clamp recordings from POMC neurons reveal that high-frequency optogenetic stimulation of ARC N/OFQ neurons produces a and robust and reversible outward current (Fig. 1J & 1N) that reverses polarity very close to the equilibrium potential for K^+ (Fig. 1L) and is associated with an increased slope conductance (Fig. 1L & 1O). These effects were markedly attenuated in the presence of the NOP receptor antagonist BAN ORL 24 (10 μM; Fig. 1K, 1M–1O; 1N: Student's t-test: $t = 2.66272$, $p < 0.03$; 3O: Student's t-test, $t = 2.38693$, $p < 0.03$). This optogenetically driven, NOP receptor-mediated increase in K^+ conductance causes a membrane hyperpolarization and cessation of firing in current clamp (Fig. 2A, 2D, 2G & 2H) that is not seen in animals injected with the eYFP blank-containing AAV (Fig. 2B, 2E, 2G & 2H) or in slices pre-treated with BAN ORL 24 (Fig. 2C, 2F–2H; 2G: one-way ANOVA/LSD, $F = 31.39$, $df = (2, 19)$, $p < 0.0001$; 2H: Kruskal-Wallis/median-notched box-and-whisker analysis, test statistic = 17.4321, $p < 0.0006$).

The in vitro effect of exogenously administered N/OFQ on this critical neuroanatomical substrate within the homeostatic energy balance circuitry is sexually differentiated and negatively modulated by estradiol in females [5, 19, 21]. We therefore set out to determine if the same held true for endogenous peptide release from ARC N/OFQ neurons. Optogenetic excitation of ARC N/OFQ neurons in slices prepared from OVX female N/OFQ-cre/eGFP-POMC mice once again elicited a sizable outward current (Fig. 3A & 3E) and increase in K^+ conductance (Fig. 3C & 3F) that was significantly diminished by E_2 pretreatment (100 nM; Fig. 3B, 3D–3F) initiated 4–5 minutes prior to photostimulation (3E: Student's t-test: $t = 2.49578$, $p < 0.03$; 3F: Student's t-test, $t = 2.94837$, $p < 0.009$).

3.2 Experiment 2: In Vitro Effects of Endogenous N/OFQ on the Excitability of Reward Encoding A_{10} Dopamine Neurons in Male and Female Mice

VTA N/OFQ neurons inhibit A_{10} dopamine neurons via a NOP receptor-mediated mechanism—Thus far we have shown that endogenous N/OFQ inhibits POMC neurons within the homeostatic energy balance circuitry by activating NOP receptors and GIRK channels in a E_2-sensitive fashion. Given that N/OFQ and its NOP receptor are expressed in A_{10} dopamine neurons [17, 33], and that exogenously administered N/OFQ inhibits A_{10} dopamine neurons and decreases dopamine release from these cells [22–24], we then wanted to ascertain whether A_{10} dopamine neurons are similarly impacted by endogenous peptide released from VTA N/OFQ nerve terminals impinging upon them. Injection of a ChR2/eYFP-containing AAV into the VTA of male N/OFQ-cre mice resulted in clear labeling of N/OFQ perikarya in the VTA as well as fiber projections that also radiated to surrounding regions (Fig. 4A & 4B). Optogenetic stimulation of these VTA N/OFQ-cre neurons reliably caused a large outward current in VTA neurons (Fig. 4C, 4D & 4H) closely apposed to N/OFQ fibers (Fig. 4B & 4C) that again was associated with increased conductance and reversed polarity near the equilibrium potential for K^+ (Fig. 4F & 4I). These effects were again abrogated by NOP receptor antagonism with BAN ORL 24 (Fig. 4E & 4G–4I; 4H: Student's t-test, $t = 2.3706$, $p < 0.04$; 4I: Student's t-test, $t = 2.13403$, $p < 0.05$). Identical findings were observed in current clamp; with photostimulation of VTA N/OFQ neurons causing membrane hyperpolarization (Fig. 5A & 5C) and a cessation of firing (Fig. 5A & 5D) that was abrogated by blockade of NOP receptors with BAN ORL 24

(Fig. 5B–5D; 5C: Student's t-test; $t = -5.30827$, $p < 0.002$; 5D: Kruskal-Wallis/median-notched box-and-whisker analysis, test statistic = 11.0199, $p < 0.005$)

The effects of endogenous N/OFQ released from nerve terminals impinging upon VTA neurons were faithfully mirrored by bath application of N/OFQ (1 μM) in mesencephalic slices prepared from male TH-cre mice injected 2–3 weeks prior with eYFP blank-containing AAV into the VTA. The overwhelming majority of TH-positive neurons in the VTA (Fig. 6A & 6C) also express eYFP injected into the same region (Figure 6B–6D). This eYFP expression was selective for A_{10} dopamine neurons as GABAergic neurons, which represent a sizable population of VTA neurons [23, 34, 35], were not labeled with the marker (Supplemental Fig. 3). N/OFQ elicits a powerful outward current in visual whole-cell patch clamp recordings from these A_{10} dopamine neurons (Fig. 6E–6G, 6K) that once again was accompanied by an increase in conductance and reversed polarity near the equilibrium potential for K^+ (Figure 6I & 6L). These effects were abolished upon NOP receptor blockade with BAN ORL 24 (Figure 6H & 6J–6L; 6K: Student's t-test, $t = 3.61837$, $p < 0.0009$; 6L: Student's t-test, $t = 3.01749$, $p < 0.005$). These effects are corroborated in current clamp recordings from A_{10} dopamine neurons, in which N/OFQ produced a large hyperpolarization (Fig. 7A & 7E) accompanied by a suppression of firing and an increase in K^+ conductance (Figure 7A, 7C & 7F). These actions were once again nullified by BAN ORL 24 (Fig. 7B & 7D–7F; 7E: Student's t-test, $t = -3.77235$, $p < 0.002$; 7F: Kruskal-Wallis/median-notched box-and-whisker analysis, test statistic = 21.4688, $p < 0.0001$). Interestingly, recordings of A_{10} dopamine neurons from long-term HFD-fed males revealed a markedly hyperpolarized RMP and reduced basal firing rate relative to those seen in chow-fed animals (Fig. 8A: Student's t-test, $t = -3.89511$, $p < 0.0005$; 8B: Student's t-test, $t = -4.26318$, $p < 0.0002$). As shown in the representative voltage traces in Figs. 8C and 8D, along with the composite data in Figs. 8E and 8F, the magnitude of the N/OFQ-induced hyperpolarization and increase in K^+ conductance did not change in the HFD-fed animals, but the duration of the hyperpolarization was considerably more prolonged (Fig. 8E: Student's t-test, $t = -1.31525$, $p < 0.20$; 8F: Student's t-test, $t = 0.254244$, $p < 0.81$).

Estradiol is an anorexigenic hormone that uncouples metabotropic $G_{i/o}$-coupled receptors from their effector K^+ channels in POMC neurons of the homeostatic energy balance circuitry [36–38]. However, it is unknown whether the same holds true for reward-encoding A_{10} dopamine neurons. Given that estradiol administered into the VTA reduces motivation for food reward [39], we set out to determine if it disrupts NOP/K+ channel coupling in A_{10} dopamine neurons. Photostimulation of VTA N/OFQ neurons induced a reversible outward current (Fig. 9A & 9E) and increased K^+ conductance (Fig. 9C & 9F) in VTA neurons receiving input during recording in slices prepared from OVX female N/OFQ-cre mice that were markedly diminished by E_2 (Fig. 9B, 9D–9F; 10E: Student's t-test, $t = 2.09844$, $p < 0.05$; 9F: Student's t-test, $t = 2.95509$, $p < 0.007$). Likewise, bath application of N/OFQ during recordings in slices prepared from OVX TH-cre females caused a reversible outward current (Fig. 10A & 10E) and increase in K^+ conductance (Fig. 10C & 10F) in A_{10} dopamine neurons that again was significantly attenuated by E_2 (Fig. 10B, 10D–10F); 10E: Student's t-test, $t = 3.10152$, $p < 0.005$; 10F: Student's t-test, $t = 3.22696$, $p < 0.003$). These effects were faithfully replicated in current clamp recordings from A_{10} dopamine neurons, in which the N/OFQ-induced membrane hyperpolarization (Fig. 11A & 11E), increase in K+

conductance (Fig. 11C) and suppression of firing (Fig. 11A & 11F) were significantly reduced by E_2 (Fig. 11B, 11D–11F; 11E: Student's t-test, $t = -2.47281$, $p < 0.03$; 11F: Kruskal-Wallis/median-notched box-and-whisker analysis, test statistic = 12.1132, $p < 0.003$).

3.3. Experiment 3: In Vivo Effects of N/OFQ on the Binge-like Consumption of Palatable Food

Focal Injection of N/OFQ Impacts Binge-eating Behavior in a Site-, Sex- and Diet-Sensitive Manner—Up to this point we have found that ARC and VTA N/OFQ neurons powerfully inhibit the excitability of critical neuroanatomical substrates within the homeostatic and hedonic energy balance circuitries; namely, anorexigenic POMC neurons and reward-encoding A_{10} dopamine neurons. We next wanted to ascertain the significance of these inhibitory actions on hedonic food consumption. N/OFQ promotes energy intake, and its hyperphagic effects are most prominent when injected into the ARC [5, 40–42]. As we and others have shown, N/OFQ inhibits A_{10} dopamine neurons and dopamine release from these cells [22–24], and the NOP receptor is an emerging target in the treatment of cocaine addiction [43]. Given that dopamine release is increased during binge feeding [14], we then set out to test the hypothesis that N/OFQ delivered directly into the VTA would differentially decrease hedonic feeding in lean and diet-induced obese wildtype mice using binge eating model of food addiction. For comparison, we also injected N/OFQ into the ARC. Limited intermittent access to HFD (one hour per day from 16:00 – 17:00) causes a rapid, dramatic escalation in consumption that is accentuated in OVX females and by diet-induced obesity (Fig. 12A; repeated measures multifactorial ANOVA/LSD: $F_{day} = 69.54$ (df = (1, 204), $p < 0.0001$), $F_{binge} = 676.90$ (df = (1, 204), $p < 0.0001$), $F_{sex} = 15.39$ (df = (1, 204), $p < 0.0002$), $F_{diet} = 11.10$ (df = (1, 204), $p < 0.002$), $F_{interaction\ (Binge\text{-}Sex)} = 11.40$ (df = (1, 204), $p < 0.001$), $F_{interaction\ (Binge\text{-}Diet)} = 1.84$ (df = (1, 204), $p < 0.18$), $F_{interaction\ (Sex\text{-}Diet)} = 0.93$ (df = (1, 204), $p < 0.34$); one-way ANOVA/LSD, $F_{ratio} = 24.11$ (df = (39, 204)$p < 0.0001$). Otherwise chow-fed males end up eating over 25% of their daily intake during that one-hour exposure, whereas obese males continuously exposed to HFD for five weeks prior to initiating the binge-feeding paradigm surpass 40%, a figure approached by both chow- and HFD-fed, hypoestrogenic OVX females (Fig. 12B; rank-transformed, repeated measures multifactorial ANOVA/LSD: $F_{binge} = 294.65$ (df = (1, 204), $p < 0.0001$), $F_{sex} = 0.86$ (df = (1, 204), $p < 0.36$), $F_{diet} = 2.44$ (df = (1, 204), $p < 0.13$), $F_{interaction\ (Binge\text{-}Sex)} = 5.47$ (df = (1, 204), $p < 0.03$), $F_{interaction\ (Binge\text{-}Diet)} = 3.03$ (df = (1, 204), $p < 0.084$), $F_{interaction\ (Sex\text{-}Diet)} = 2.58$ (df = (1, 204), $p < 0.12$); one-way ANOVA/LSD, $F_{ratio} = 48.50$ (df = (7, 204), $p < 0.0001$). Both lean and in particular obese males exhibited a significant reduction in cumulative chow consumption during the remaining 23 hours (Fig. 12C; repeated measures multifactorial ANOVA/LSD: $F_{binge} = 30.50$ (df = (1, 204), $p < 0.0001$), $F_{sex} = 11.01$ (df = (1, 204), $p < 0.002$), $F_{diet} = 21.04$ (df = (1, 204), $p < 0.0001$), $F_{interaction\ (Binge\text{-}Sex)} = 76.68$ (df = (1, 204), $p < 0.0001$), $F_{interaction\ (Binge\text{-}Diet)} = 29.50$ (df = (1, 204), $p < 0.0001$), $F_{interaction\ (Sex\text{-}Diet)} = 0.01$ (df = (1, 204), $p < 0.92$); one-way ANOVA/LSD, $F_{ratio} = 27.52$ (df = (7, 204), $p < 0.0001$). Similar degrees of this rampant binge feeding were observed irrespective of when the HFD exposure occurred (Fig. 12D; repeated measures one-way ANOVA/LSD, df = (2, 72), $F_{ratio} = 0.75$, $p < 0.48$).

Intra-VTA delivery of N/OFQ (0.3 nmol) decreased binge feeding in obese males, and this effect was appreciably attenuated by co-administration of the NOP receptor antagonist UFP-101 (10 nmol). N/OFQ was without effect in lean males (Fig. 13A; repeated measures one-way ANOVA/LSD, df = (4, 132), $F_{ratio} = 7.48$, $p < 0.0001$). By contrast, N/OFQ administered directly into the ARC, where it acts to inhibit anorexigenic POMC neurons, enhanced consumption (Fig. 13B; Student's t-test, $t = -3.15313$, $p < 0.003$). Given that estradiol uncouples the NOP receptor from its effector K^+ channels, we then endeavored to evaluate the interaction between N/OFQ and the steroid in OVX females. As shown in Fig. 13C, N/OFQ injected into the VTA suppressed binge feeding in sesame oil-treated (1 mL/kg; s.c.) OVX females, regardless of whether they were lean or obese. EB (20 μg/kg; s.c.) *per se* also reduced the binge-like escalation in both lean and obese females, However, most interesting was the fact that it counteracted the inhibitory effect of N/OFQ, which was most prominent in obese females (repeated measures multifactorial ANOVA/LSD: $F_{EB} = 0.66$ (df = (1, 192), $p < 0.42$), $F_{N/OFQ} = 0.05$ (df = (1, 192), $p < 0.83$), $F_{diet} = 1.88$ (df = (1, 192), $p < 0.18$), $F_{interaction\ (EB\text{-}N/OFQ)} = 28.26$ (df = (1, 192), $p < 0.0001$), $F_{interaction\ (EB\text{-}Diet)} = 1.22$ (df = (1, 192), $p < 0.28$), $F_{interaction\ (N/OFQ\text{-}Diet)} = 0.21$ (df = (1, 192), $p < 0.65$), $F_{interaction\ (EB\text{-}N/OFQ\text{-}Diet)} = 3.80$ (df = (1, 192), $p < 0.06$); one-way ANOVA/LSD, $F_{ratio} = 5.84$ (df = (7, 192), $p < 0.0001$).

4. DISCUSSION

The results of the present study demonstrate that N/OFQ profoundly impacts both the homeostatic and hedonic energy balance circuits to alter the binge-like consumption of palatable food in a manner that is site-specific, influenced by adiposity, and negatively modulated by estradiol in females. These findings are based on the following observations: 1) N/OFQ elicits an outward current in ARC POMC neurons and A_{10} dopamine neurons in the VTA that is virtually abolished by NOP receptor blockade, 2) this outward current is associated with a membrane hyperpolarization and a resultant decrease in firing, which is diminished by estradiol in females and enhanced under conditions of diet-induced obesity in males, 3) the outward current and hyperpolarization caused by exogenous N/OFQ in A_{10} dopamine neurons is recapitulated by photo-stimulation of VTA N/OFQ neurons, which again is blunted by estradiol, 4) focal injection of N/OFQ into the ARC amplifies binge eating, whereas in the VTA the opposite effect occurs, and 5) the dampening effect of intra-VTA N/OFQ on the striking binge-like escalation in palatable food ingestion is heightened by diet-induced obesity in males and nullified by estradiol in females.

We have demonstrated that pronounced inhibitory neurotransmission occurring at ARC N/OFQ/POMC and VTA N/OFQ/A_{10} dopamine synapses arises from the activation of the NOP receptors. The N/OFQ-induced hyperpolarization and underlying outward current seen in POMC neurons is abrogated by GIRK channel blockers such as Ba^{2+} and tertiapin [19, 31, 44]. In both POMC and A_{10} dopamine neurons the reversal potential associated with the N/OFQ-induced hyperpolarization and outward current is dependent on the extracellular K^+ concentration [23, 44]. Collectively, these observations are consistent with the fact that N/OFQ activates GIRK channels in the dorsal raphe [45], locus coeruleus [46], periaqueductal gray [47], suprachiasmatic nucleus [48], VMN [5, 49, 50], nucleus raphe magnus [51] and in cultured tuberomammillary neurons [52]. We also found that the NOP

receptor-mediated activation of GIRK channels in POMC and A_{10} dopamine neurons caused by endogenously released N/OFQ from ARC and VTA neurons, respectively, is physiologically antagonized by estradiol. This finding aligns with other examples of estrogenic uncoupling of metabotropic, $G_{i/o}$-coupled receptors (e.g., μ-opioid, $GABA_B$, CB1) from their effector GIRK channels [36–38]. The hyperpolarization elicited by K^+ efflux through GIRK channels suppresses neuronal firing in a profound and powerful way [53, 54]. Therefore, it stands to reason that the estradiol-induced negative modulation of NOP/GIRK coupling can dramatically impact the excitability of POMC and A_{10} dopamine neurons and thus the function of the homeostatic and hedonic energy balance circuitries.

Synapses formed between upstream SF-1-containing neurons in the VMN and POMC neurons in the ARC represent a critical anorexigenic synapse within the homeostatic energy balance circuitry [5, 6, 27, 55]. N/OFQ inhibits excitatory neurotransmission at this synapse pleiotropically in three ways: 1) it hyperpolarizes and decreases the firing rate of VMN SF-1 neurons [5, 50], 2) it presynaptically inhibits glutamate release at synapses formed with POMC neurons [5, 19] and 3) it hyperpolarizes and thereby inhibits POMC somas in the ARC [5, 19, 21]. All three of these effects of exogenous N/OFQ are sexually differentiated; with males being more sensitive than females [5]. The activity of these two cell types are also influenced by peripheral hormones such as leptin [56–58], insulin [59–62] and ghrelin [63], neuromodulators such as endocannabinoids [7, 27, 64, 65] and neuropeptides such as pituitary adenylyl cyclase-activating polypeptide (PACAP) [30, 66]. Thus, it is clear that this synapse is an integrative cornerstone in the neuronal and hormonal regulation of the homeostatic energy balance circuitry.

The present study also demonstrates that intermittent exposure to a palatable HFD dramatically escalates consumption in a binge-like fashion, and that N/OFQ dichotomously regulates this binge eating through its inhibitory actions within the homeostatic and hedonic energy balance circuitries. On one hand, focal delivery of N/OFQ into the ARC potentiates binge feeding, whereas on the other hand delivery into the VTA reduces it. This finding clearly indicates that N/OFQ-induced inhibition of POMC neurons within the homeostatic energy balance circuitry can influence hedonic binge feeding. On the other hand, A_{10} dopaminergic inputs into the nucleus accumbens increase the incentive salience for palatable food and other reinforcers [11], whereas those inputs into the medial prefrontal cortex might play a role in regulating food-seeking behavior and impulsivity [13]. Dopamine release in the nucleus accumbens is increased during binge feeding [14], which can also be exacerbated by chronic stress and associated with heightened food addiction score and increases in μ-opioid and dopamine D2 receptor expression in the nucleus accumbens [67]. In addition, dopamine replacement therapy promotes binge eating and food addiction in Parkinson’s patients and in experimental animal models of Parkinsonism [68, 69]. Our findings reveal that in A_{10} dopamine neurons, a markedly hyperpolarized RMPis accompanied by a reduction in the basal firing rate under conditions of diet-induced obesity in males. This may reflect a state of anhedonia that is associated with heightened binge feeding [70, 71]. Our present results also demonstrate that NOP receptor-mediated inhibition of A_{10} dopamine neurons, which is much more prolonged under conditions of diet-induced obesity, accounts, at least in part, for the blunted binge feeding observed in these animals when N/OFQ is injected into the VTA. This adds substantially to our understanding of how

neuropeptides regulate compulsive binge feeding behavior. Like N/OFQ in the present study, ghrelin promotes binge eating and the growth hormone secretagogue receptor is required for its full expression [15]. By contrast, PACAP administered into the nucleus accumbens decreases the hedonic consumption of palatable food [72, 73]. Interestingly, systemic administration of the NOP receptor antagonist SB 61211 decreases binge feeding in male and female mice [74], whereas in the present study we found that blockade of NOP receptors in the VTA abrogated the reduction in this behavior caused by N/OFQ delivered into the same region. Thus, the N/OFQ-induced inhibition of critical anorexigenic substrates within the homeostatic energy balance circuitry might actually play a more prominent role in the NOP receptor-mediated regulation of hedonic feeding than originally thought.

Our findings also point to a sex difference in the NOP receptor mediated reduction in binge feeding behavior. For example, N/OFQ decreases binge feeding in both lean and obese, hypoestrogenic females, whereas in males this occurs only in those that are obese. This is in agreement with sex differences in binge feeding driven by relaxin-family peptide-3 receptors in the paraventricular nucleus (more extensive in females) and orexin neurons in the dorsomedial nucleus and lateral hypothalamus (greater numbers in females) [75, 76]. Diet-induced obesity in males increases the excitability of ARC N/OFQ neurons as well as the sensitivity of postsynaptic targets like the POMC neurons receiving input from these cells [5, 20]. The results of the present study demonstrates the same holds true for VTA N/OFQ neurons and the A_{10} dopamine neurons receiving input from them, which could then account for the dampening effect of N/OFQ on binge eating when administered into this region. Lastly, our findings are also consistent with other examples of how these neurons mediate drug-induced reward in a sexually differentiated manner. Indeed, estradiol enhances dopamine release in the nucleus accumbens in response to cocaine and amphetamine, as well as their respective locomotor effects and rate of behavioral sensitization, in female but not male rodents [77, 78].

In the present study, we used a modified binge-feeding paradigm as a model for food addiction. While food addiction *per se* is not currently recognized by the DSM, emerging evidence indicates that obesity and associated co-morbidities like insulin resistance can increase vulnerability to food and drug addiction. For example, cross-lagged panel analyses have revealed that overweight and obese men are more likely to be daily tobacco smokers and engage in hazardous cannabis use [79]. In addition, Otsuka Long Evans Tokushima Fatty rats that are prone to binge eating exhibit heightened cocaine craving after four weeks of restricted access to a palatable diet [80]. Similarly, food addiction is associated with elevated body mass index, and its prevalence is reported to be highest in individuals with bulimia nervosa [81]. Food addiction and impulsivity are also significant predictors of elevated BMI and obesity in individuals with type 2 diabetes [82]. Moreover, women are ~3X more likely to develop food addiction than their male counterparts [83]. Collectively, these factors may help explain why only obese males exhibit more rampant binge feeding, whereas lean and obese females are equally prone.

In conclusion, the present results provide compelling support for the idea that ARC and VTA N/OFQ neurons powerfully inhibit anorexigenic POMC neurons and reward-encoding A_{10} dopamine neurons, respectively, in a manner that is negatively modulated by estradiol in

females. This in turn leads to equally powerful yet disparate influences of these different populations of N/OFQ neurons on binge feeding behavior that are sexually differentiated as well as diet- and estradiol-sensitive. These findings have important implications for the pathogenesis of food addiction.

Supplementary Material

Refer to Web version on PubMed Central for supplementary material.

Funding Sources

This study was supported by PHS Grant DA024314 and intramural funding from Western University of Health Sciences.

Abbreviations and Their Corresponding Key Terms and Phrases

AAV	adeno-associated viral vector
aCSF	artificial cerebral spinal fluid
ARC	hypothalamic arcuate nucleus
ChR2	channel rhodopsin-2
E_2	17β-estradiol
EB	estradiol benzoate
eGFP	enhanced green fluorescent protein
eYFP	enhanced yellow fluorescent protein
GIRK	G-protein coupled inwardly-rectifying K+
HFD	high-fat-diet
I/V	current-voltage relationship
N/OFQ	nociceptin/orphanin FQ
NOP	nociceptin opioid peptide
OVX	ovariectomized
PACAP	pituitary adenylyl cyclase-activating polypeptide
POMC	proopiomelanocortin
RMP	resting membrane potential
SF-1	steroidogenic factor 1
TH	tyrosine hydroxylase
TTX	Tetrodotoxin

UFP-101	[Nphe^{1},Arg^{14},Lys^{15}]Nociceptin-NH_2, NOP receptor antagonist
VMN	hypothalamic ventromedial nucleus
VTA	ventral tegmental area

REFERENCES

[1]. Di Marzo V, Ligresti A, Cristino L The endocannabinoid system as a link between homeostatic and hedonic pathways involved in energy balance regulation. Int. J. Obesity 2009,33:S18–S24.

[2]. Berthoud H-R The neurobiology of food intake in an obesogenic environment. Proc. Nutr. Soc 2012,71:478–87. [PubMed: 22800810]

[3]. Fordahl SC, Jones SR High-fat-diet induced deficits in dopamine terminal function are reversed by restoring insulin signaling. ACS Chem Neurosci 2017,8:290–9. [PubMed: 27966885]

[4]. Volkow ND, Wise RA, Baler R The dopamine motive system: implications for drug and food addiction. Nat Rev Neurosci. 2017,18:741–52. [PubMed: 29142296]

[5]. Hernandez J, Fabelo C, Perez L, Moore C, Chang R, Wagner EJ Nociceptin/orphanin FQ modulates energy homeostasis through inhibition of neurotransmission at VMN SF-1/ARC POMC synapses in a sex- and diet-dependent manner. Biol. Sex Diff 2019,10,doi:10.1186/s13293-019-0220-3.

[6]. Krashes MJ, Shah BP, Madara JC, Olson DP, Strochlic DE, Garfield AS, et al. An excitatory paraventricular nucleus to AgRP neuron circuit that drives hunger. Nature. 2014,507:238–42. [PubMed: 24487620]

[7]. Conde K, Fabelo C, Krause WC, Propst R, Goethel J, Fischer D, et al. Testosterone rapidly augments retrograde endocannabinoid signaling in proopiomelanocortin neurons to suppress glutamatergic input from steroidogenic factor 1 neurons via upregulation of diacylglycerol lipase-α. Neuroendocrinology. 2017,105:341–56. [PubMed: 27871072]

[8]. Kalivas PW, Duffy P Sensitization to repeated morphine injection in the rat: possible involvement of A_{10} dopamine neurons. J. Pharmacol. Exp. Ther 1987,241:204–12. [PubMed: 3572784]

[9]. Denis RGP, Joly-Amado A, Webber E, Langlet F, Schaeffer M, Padilla SL, et al. Palatability can drive feeding independent of AgRP neurons. Cell Metabolism. 2015,22:646–57. [PubMed: 26278050]

[10]. Durst M, Konczol K, Balazsa T, Eyre MD, Toth ZE Reward-representing D1-type neurons in the medial shell of the accumbens nucleus regulate palatable food intake. Int. J. Obesity 2019:917–27.

[11]. Robinson TE, Berridge KC The incentive sensitization theory of addiction: some current issues. Phil. Trans. R. Soc. B 2008,363:3137–46. [PubMed: 18640920]

[12]. Carlin JL, McKee SE, Hill-Smith T, Grissom NM, George R, Lucki I, et al. Removal of high-fat diet after chronic exposure drives binge behavior and dopaminergic dysregulation in female mice. Neuroscience. 2016,326:170–9. [PubMed: 27063418]

[13]. Warthen DM, Lambeth PS, Ottolini M, Shi Y, Barker BS, Gaykema RP, et al. Activation of pyramidal neurons in mouse medial prefrontal cortex enhances food-seeking behavior while reducing impulsivity in the absence of an effect on food intake. Front. Behav. Neurosci 2016,10,doi:10.3389/fnbeh.2016.00063.

[14]. Avena NM, Bocarsly ME Dysregulation of brain reward systems in eating disorders: neurochemical information from animal models of binge eating, bulimia nervosa, and anorexia nervosa. Neuropharmacology. 2012,63:87–96. [PubMed: 22138162]

[15]. Valdivia S, Cornejo MP, Reynaldo M, De Francesco PN, Perello M Escalation in high fat intake in a binge eating model differentially engages dopamine neurons of the ventral tegmental area and requires ghrelin signaling Psychoneuroendocrinology. 2015,60:206–16.

[16]. Ikeda K, Watanabe M, Ichikawa T, Kobayashi T, Yano R, Kumanishi T Distribution of prepro-nociceptin/orphanin FQ mRNA and its receptor mRNA in developing and adult mouse central nervous systems. J. Comp. Neurol 1998,399:139–51. [PubMed: 9725707]

[17]. Norton CS, Neal CR, Kumar S, Akil H, Watson SJ Nociceptin/orphanin FQ and opiod receptor-like receptor mRNA expression in dopamine systems. J. Comp. Neurol 2002,444:358–68. [PubMed: 11891648]

[18]. Sinchak K, Romeo HE, Micevych PE Site-specific estrogen and progestin regulation of orphanin FQ/nociceptin and nociceptin opioid receptor mRNA expression in the female rat limbic hypothalamic system. J. Comp. Neurol 2006,496:252–68. [PubMed: 16538678]

[19]. Borgquist A, Kachani M, Tavitian N, Sinchak K, Wagner EJ Estradiol negatively modulates the pleiotropic actions of orphanin FQ/nociceptin at proopiomelanocortin synapses. Neuroendocrinology. 2013,98:60–72. [PubMed: 23735696]

[20]. Jais A, Paeger L, Sotelo-Hitschfeld T, Bremser S, Prinzensteiner M, Klemm P, et al. $PNOC^{ARC}$ neurons promote hyperphagia and obesity upon high-fat feeding. Neuron. 2020,106:1–17. [PubMed: 32272061]

[21]. Conde K, Meza C, Kelly MJ, Sinchak K, Wagner EJ Estradiol rapidly attenuates ORL-1 receptor-mediated inhibition of proopiomelanocortin neurons via G_q-coupled, membrane-initiated signaling. Neuroendocrinology. 2016,103:787–805. [PubMed: 26765570]

[22]. Murphy NP, Maidment NT Orphanin FQ/nociceptin modulation of mesolimbic dopamine transmission determined by microdialysis. J. Neurochem 1999,73:179–86. [PubMed: 10386969]

[23]. Zheng F, Grandy DK, Johnson SW Actions of orphanin FQ/nociceptin on rat ventral tegmental area neurons *in vitro*. Br. J. Pharmacol 2002,136:1065–71. [PubMed: 12145107]

[24]. Murphy NP, Tan AM, Lam HA, Maidment NT Nociceptin/orphanin FQ modulation of rat midbrain dopamine neurons in primary culture. Neuroscience. 2004,127:929–40. [PubMed: 15312905]

[25]. Hardaway JA, Halladay LR, Mazzone CM, Pati D, Bloodgood DW, Kim M, et al. Central Amygdala *prepronociceptin*-expressing neurons mediate food consumption and reward. Neuron. 2019,102:1037–52. [PubMed: 31029403]

[26]. Qiu J, Bosch MA, Meza C, Navarro U-V, Nestor CC, Wagner EJ, et al. Estradiol protects proopiomelanocortin neurons against insulin resistance. Endocrinology. 2018,159:647–64. [PubMed: 29165691]

[27]. Fabelo C, Hernandez J, Chang RS, S., Alicea N, , Tian S, et al. Endocannabinoid signaling at hypothalamic steroidogenic factor-1/proopiomelanocortin synapses is sex- and diet-sensitive. Front. Mol. Neurosci 2018,11,doi:10.3389/fnmol.201800214.

[28]. Mattis J, Tye KM, Ferenczi EA, Ramakrishnan C, O'Shea DJ, Prakash R, et al. Principles for applying optogenetic tools derived from direct comparitive analysis of microbial opsins. Nat Methods. 2012,9:159–72.

[29]. Qiu J, Nestor CC, Zhang C, Padilla SL, Palmiter RD, Kelly MJ, et al. High-frequency stimulation-induced peptide release synchronizes arcuate kisspeptin neurons and excites GnRH neurons. eLife. 2016,5:DOI: 10.7554/eLife.16246.

[30]. Chang R, Hernandez J, Gastelum C, Guadagno K, Perez L, Wagner EJ Pituitary adenylate cyclase-activating polypeptide excites proopiomelanocortin neurons: implications for the regulation of energy homeostasis. Neuroendocrinology. 2020:doi: 10.1159/000506367.

[31]. Farhang B, Pietruszewski L, Lutfy K, Wagner EJ The role of the NOP receptor in regulating food intake, meal pattern, and the excitability of proopiomelanocortin neurons. Neuropharmacology. 2010,59:190–200. [PubMed: 20510254]

[32]. Rospond B, Szpigiel J, Sadakierska-Chudy A, Filip M Binge eating in pre-clinical models. Pharmacol. Rep 2015,67:504–12. [PubMed: 25933962]

[33]. Maidment NT, Chen Y, Tan AM, Murphy NP, Leslie FM Rat ventral midbrain dopamine neurons express the orphanin FQ/nociceptin receptor ORL-1. Neuroreport. 2002,13:1137–40. [PubMed: 12151756]

[34]. Steffensen SC, Svingos AL, Pickel VM, Henriksen SJ Electrophysiological characterization of GABAergic neurons in the ventral tegmental area. J. Neurosci 1998,18:8003–15. [PubMed: 9742167]

[35]. Brown MTC, Tan KR, E.C., O. C., Nikonenko, I., Muller, D., Luscher, C. Ventral tegmental area GABA projections pause accumbal cholinergic interneurons to enhance associative learning. Nature. 2012,492:452–6. [PubMed: 23178810]

[36]. Lagrange AH, Ronnekleiv OK, Kelly MJ The potency of μ-opioid hyperpolarization of hypothalamic arcuate neurons is rapidly attenuated by 17β-estradiol. J. Neurosci 1994,14:6196–204. [PubMed: 7931572]

[37]. Qiu J, Bosch MA, Tobias SC, Grandy DK, Scanlan TS, Rønnekleiv OK, et al. Rapid signaling of estrogen in hypothalamic neurons involves a novel G-protein-coupled estrogen receptor that activates protein kinase C. J. Neurosci 2003,23:9529–40. [PubMed: 14573532]

[38]. Mela V, Vargas A, Meza C, Kachani M, Wagner EJ Modulatory influences of estradiol and other anorexigenic hormones on metabotropic, Gi/o-coupled receptor function in the hypothalamic control of energy homeostasis. J. Steroid Biochem. Mol. Biol 2016,160:15–26. [PubMed: 26232394]

[39]. Richard JE, Lopez-Ferreras L, Anderberg RH, Olandersson K, Skibicka KP Estradiol is a critical regulator of food-reward behavior. Psychoneuroendocrinology. 2017,78:193–202. [PubMed: 28214679]

[40]. Pomonis JD, Billington CJ, Levine AS Orphanin FQ, agonist of the orphan opioid receptor, stimulates feeding in rats. Neuroreport. 1996,8:369–71. [PubMed: 9051812]

[41]. Stratford TR, Holahan MR, Kelley AE Injections of nociceptin into the nucleus accumbens shell or ventromedial hypothalamic nucleus increase food intake. Neuroreport. 1997,8:423–6. [PubMed: 9080421]

[42]. Polidori C, de Caro G, Massi M The hyperphagic effect of nociceptin/orphanin FQ in rats. Peptides. 2000,21:1051–62. [PubMed: 10998540]

[43]. Lutfy K, Zaveri NT The nociceptin receptor as an emerging molecular target for cocaine addiction. Prog. Mol. Biol. Transl. Sci 2016,137:149–81. [PubMed: 26810001]

[44]. Wagner EJ, Rønnekleiv OK, Grandy DK, Kelly MJ The peptide orphanin FQ inhibits β-endorphin neurons and neurosecretory cells in the hypothalamic arcuate nucleus by activating an inwardly-rectifying K^+ conductance. Neuroendocrinology. 1998,67:73–82. [PubMed: 9508037]

[45]. Vaughan CW, Christie MJ Increase by the ORL_1 receptor (opioid receptor-like1) ligand, nociceptin, of inwardly rectifying K conductance in dorsal raphe neurones. Br. J. Pharmacol 1996,117:1609–11. [PubMed: 8732266]

[46]. Connor M, Vaughan CW, Chieng B, Christie MJ Nociceptin receptor coupling to a potassium conductance in rat locus coeruleus neurones *in vitro*. Br. J. Pharmacol 1996,119:1614–8. [PubMed: 8982509]

[47]. Vaughan CW, Ingram SL, Christie MJ Actions of the ORL_1 receptor ligand nociceptin on membrane properties of rat periaqueductal gray neurons *in vitro*. J. Neurosci 1997,17:996–1003. [PubMed: 8994054]

[48]. Allen CN, Jiang Z-G, Teshima K, Darland T, Ikeda M, Nelson CS, et al. Orphanin-FQ/Nociceptin (OFQ/N) modulates the activity of suprachiasmatic nucleus neurons. J. Neurosci 1999,19:2152–60. [PubMed: 10066268]

[49]. Emmerson PJ, Miller RJ Pre- and postsynaptic actions of opioid and orphan opioid agonists in the rat arcuate nucleus and ventromedial hypothalamus *in vitro*. J. Physiol. (Lond.) 1999,517:431–45. [PubMed: 10332093]

[50]. Chee MJ, Price CJ, Statnick MA, Colmers WF Nociceptin/orphanin FQ suppresses the excitability of neurons in the ventromedial nucleus of the hypothalamus. J. Physiol. (Lond.) 2011,589:3103–14. [PubMed: 21502286]

[51]. Pan ZZ, Hirakawa N, Fields HL A cellular mechanism for the bidirectional pain-modulating actions of orphanin FQ/nociceptin. Neuron. 2000,26:515–22. [PubMed: 10839369]

[52]. Bajic D, Hoang QV, Nakajima S, Nakajima Y Dissociated histaminergic neuron cultures from the tuberomammillary nucleus of rats: culture methods and ghrelin effects. J. Neurosci Methods 2004,132:177–84. [PubMed: 14706715]

[53]. Rudy B Diversity and ubiquity of K channels. Neuroscience. 1988,25:729–49. [PubMed: 2457185]

[54]. Hille B Potassium Channels and Chloride Channels In: Hille B, ed. Ionic Channels of Excitable Membranes. 2 ed Sunderland, Mass: Sinauer Associates, Inc.; 1992 p. 115–39.

[55]. Lindberg D, Chen P, Li C Conditional viral tracing reveals that steroidogenic factor 1-positive neurons of the dorsomedial subdivision of the ventromedial hypothalamus project to the

autonomic centers of the hypothalamus and hindbrain. J. Comp. Neurol 2013,521:3167–90. [PubMed: 23696474]

[56]. Cowley MA, Cone RD, Enriori P, Louiselle I, Williams SM, Evans AE Electrophysiological actions of peripheral hormones on melanocortin neurons. Ann. NY Acad. Sci 2003,994:175–86. [PubMed: 12851314]

[57]. Dhillon H, Zigman JM, Ye C, Lee CE, McGovern RA, Tang V, et al. Leptin directly activates SF1 neurons in the VMH, and this action by leptin is required for normal body-weight homeostasis. Neuron. 2006,49:191–203. [PubMed: 16423694]

[58]. Qiu J, Fang Y, Rønnekleiv OK, Kelly MJ Leptin excites proopiomelanocortin neurons via activation of TRPC channels. J. Neurosci 2010,30:1560–5. [PubMed: 20107083]

[59]. Klöckener T, Hess S, Belgardt BF, Paeger L, Verhagen LAW, Husch A, et al. High-fat feeding promotes obesity via insulin receptor/PI3K-dependent inhibition of SF-1 VMH neurons. nature neuroscience. 2011,14:911–8. [PubMed: 21642975]

[60]. Qiu J, Zhang C, Borgquist A, Nestor CC, Smith AW, Bosch MA, et al. Insulin excites anorexigenic proopiomelanocortin neurons via activation of canonical transient receptor potential channels. Cell Metabolism. 2014,19:682–93. [PubMed: 24703699]

[61]. Dodd GT, Michael NJ, Lee-Young RS, Mangiafico SP, Pryor JT, Munder AC, et al. Insulin regulates POMC neuronal plasticity to control glucose metabolism. eLife. 2018,7:10.7554/eLife.38704.

[62]. He Z, Gao Y, Lieu L, Afrin S, Guo H, Williams KW Acute effects of zinc and insulin on arcuate anorexigenic proopiomelanocortin neurons. Br. J. Pharmacol 2019,176:725–36. [PubMed: 30521677]

[63]. Tong Q, Ye C-P, Jones JE, Elmquist JK, Lowell BB Synaptic release of GABA by AgRP neurons is required for normal regulation of energy balance. nature neuroscience. 2008,11:998–1000. [PubMed: 19160495]

[64]. Kim KW, Jo Y-H, Zhao L, Stallings NR, Chua SC, Parker KL Steroidogenic factor 1 regulates expression of the cannabinoid receptor 1 in the ventromedial hypothalamic nucleus. Mol. Endocrinol 2008,22:1950–61. [PubMed: 18511494]

[65]. Cardinal P, André C, Quarta C, Bellocchio L, Clark S, Elie M, et al. CB1 cannabinoid receptor in SF1-expressing neurons of the ventromedial hypothalamus determines metabolic responses to diet and leptin. Mol. Metab 2014,3:705–16. [PubMed: 25352999]

[66]. Mounien L, Bizet P, Boutelet I, Gourcerol G, Fournier A, Vaudry H, et al. Pituitary adenylate cyclase-activating polypeptide directly modulates the activity of proopiomelanocortin neurons in the rat arcuate nucleus. Neuroscience. 2006,143:155–63. [PubMed: 16962718]

[67]. Wei N-L, Quan Z-F, Zhao T, Yu X-D, Xie Q, Zeng J, et al. Chronic stress increases susceptibility to food addiction by increasing the levels of DR2 and MOR in the nucleus accumbens. Neuropsychiatr. Dis. Treat 2019,15:1211–29. [PubMed: 31190828]

[68]. de Chazeron I, Durif F, Chereau-Boudet I, Fantini ML, Marques A, Derost P, et al. Compulsive eating behaviors in Parkinson's disease. Eat. Weight Disord 2019,24:421–9. [PubMed: 30715681]

[69]. Mineo D, Cacace F, Mancini M, Vannelli A, Campanelli F, Natale G, et al. Dopamine drives binge-like consumption of a palatable food in experimental Parkinsonism. Mov. Disord 2019,34:821–31. [PubMed: 31002748]

[70]. Keranen A-M, Rasinaho E, Hakko H, Savolainen M, Lindeman S Eating behavior in obese and overweight persons with and without anhedonia. Appetite. 2010,55:726–9. [PubMed: 20801180]

[71]. Qu N, He Y, Wang C, Xu P, Yang Y, Cai X, et al. A POMC-originated circuit regulates stress-induced hypophagia, depression, and anhedonia. Mol. Psychiatry 2020,25:1006–21. [PubMed: 31485012]

[72]. Hurley MM, Maunze B, Block ME, Frenkel MM, Reily MJ, Kim E, et al. Pituitary adenylate-cyclase activating polypeptide regulates hunger- and palatability-induced binge eating. Front Neurosci. 2016,10.

[73]. Hurley MM, Robble MR, Callan G, Choi S, Wheeler RA Pituitary adenylate cyclase-activiating polypeptide (PACAP) acts in the nucleus accumbens to reduce hedonic drive. Int. J. Obesity 2019,43:928–32.

[74]. Hardaway JA, Jensen J, Kim M, Mazzone CM, Sugam JA, Diberto JF, et al. Nociceptin receptor antagonist SB 61211 decreases high fat diet binge eating. Behav. Brain Res 2016,307:25–34. [PubMed: 27036650]

[75]. Kania A, Szlaga A, Sambak P, Gugula A, Blasiak E, Vittoria M, et al. RLN3/RXFP3 signaling in the PVN inhibits magnocellular neurons via M-like current activation and contributes to binge eating behavior. J. Neurosci 2020,40.

[76]. Freeman LR, Bentzley BS, James MH, Aston-Jones G Sex differences in demand for highly palatable foods: role of the orexin system. Int. J. Neuropsychopharmacol 2020:DOI: 10.1093/ijnp/pyaa040.

[77]. Becker JB, Rudick CN Rapid effects of estrogen or progesterone the amphetamine-induced increase in striatal dopamine are enhanced by estrogen priming: a microdialysis study. Pharmacol. Biochem. Behav 1999,64:53–571756. [PubMed: 10494997]

[78]. Hu M, Becker JB Effects of sex and estrogen on behavioral sensitization to cocaine in rats. J. Neurosci 2003,23:693–9. [PubMed: 12533629]

[79]. N'Goran AA, Studer J, Deline S, Henchoz Y, Baggio S, Mohler-Kuo M, et al. Bidirectional relationship between the body mass index and substance use in young men. Subst. Abus 2015,37:190–6. [PubMed: 25774652]

[80]. Barnea R, Bekker L, Zifman N, Marco A, Yadid G, Weller A Trait and state binge eating predispose towards cocaine craving. Addict. Biol 2015,doi: 10.1111/adb.12315.

[81]. Gearhardt AN, Boswell RG, White MA The association of "food addiction" with disordered eating and body mass index. Eat. Behav 2014,15:427–33. [PubMed: 25064294]

[82]. Raymond K-L, Lovell GP Food addiction symptomatology, impulsivity, mood, and body mass index in people with type two diabetes. Appetite. 2015,95:383–9. [PubMed: 26232140]

[83]. Yu Z, Indelicato NA, Fuglestad P, Tan M, Bane L Sex differences in disordered eating and food addiction among college students. Appetite. 2018,129:12–8. [PubMed: 29935291]

Highlights

- Nocieptin/orphanin FQ inhibits the excitability of proopiomelanocortin and A_{10} dopamine neurons
- Nocieptin/orphanin FQ dichotomously regulates binge-feeding behavior in site-specific ways
- Estradiol attenuates these effects of nocieptin/orphanin FQ in females
- Diet-induced obesity potentiates nocieptin/orphanin FQ-induced reductions in binge-eating in males

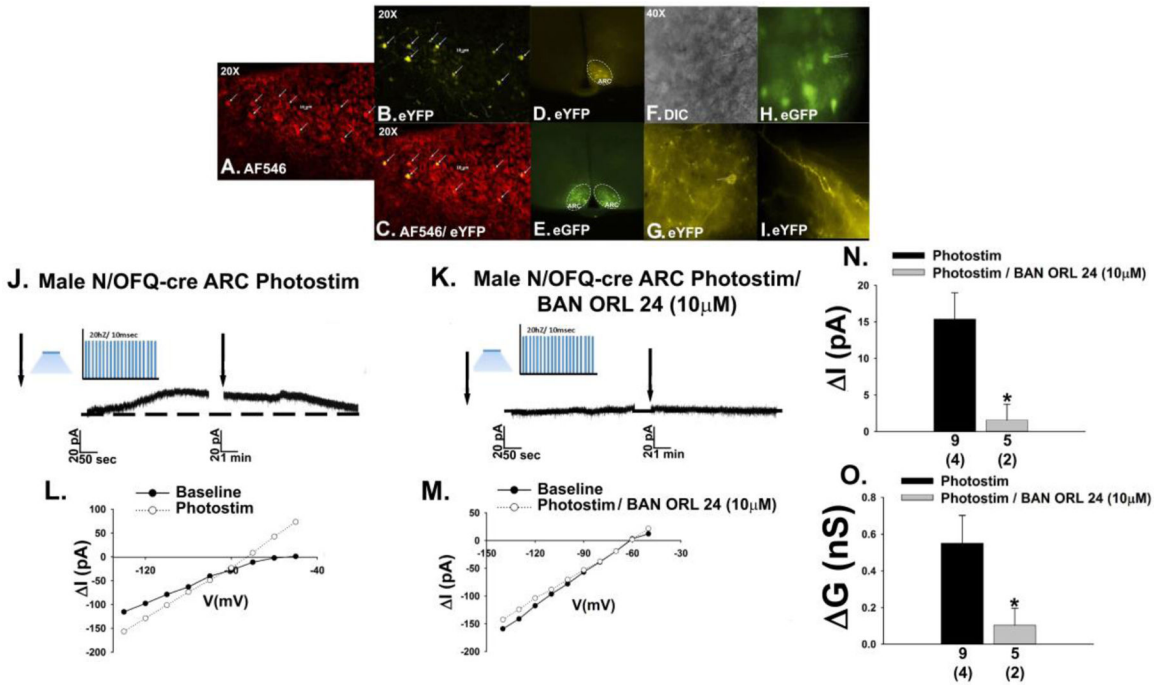

Fig. 1.

Photostimulation (photostim) of ARC N/OFQ neurons inhibits POMC neurons in male N/OFQ-cre/eGFP-POMC mice. **A**, N/OFQ immunostaining in the ARC visualized with AF546. **B**, eYFP ChR2 reporter signal in the cells in **A**. **C**, Composite overlay (20X). **D & E**, Low power images of the eYFP ChR2 reporter signal in ARC N/OFQ neurons juxtaposed with the eGFP reporter signal in ARC POMC neurons. **F**, DIC image (40X) of a recorded ARC neuron. **G**, eYFP/ChR2-labelled N/OFQ fibers and perikaryal in the immediate vicinity of the cell in **F**. **H**, eGFP POMC reporter signal in the cell in **F**. **I**, Prominent N/OFQ fiber labelling and a conspicuous absence of N/OFQ somas in the VMN. **J**, Optogenetic stimulation of ARC N/OFQ neurons elicits a robust and reversible outward current (n = 9) in the POMC neuron shown in **H** that is blocked by the NOP receptor antagonist BAN ORL 24 (10 μM; **K**; n = 5). **L**, I/V relationships generated prior to and following photostimulation show the increased slope conductance that again is antagonized by BAN ORL 24 (**M**). **N & O**, Composite bar graphs illustrating the NOP receptor-mediated outward current and increase in slope conductance. Bars represent means and lies 1 SEM. Numbers above parenthesis in bar graphs are indicative of the number of cells recorded for that treatment, while numbers in parenthesis are indicative of the number of animals used for that treatment. *, $p < 0.05$, relative to Photostimulation alone, Student's t test

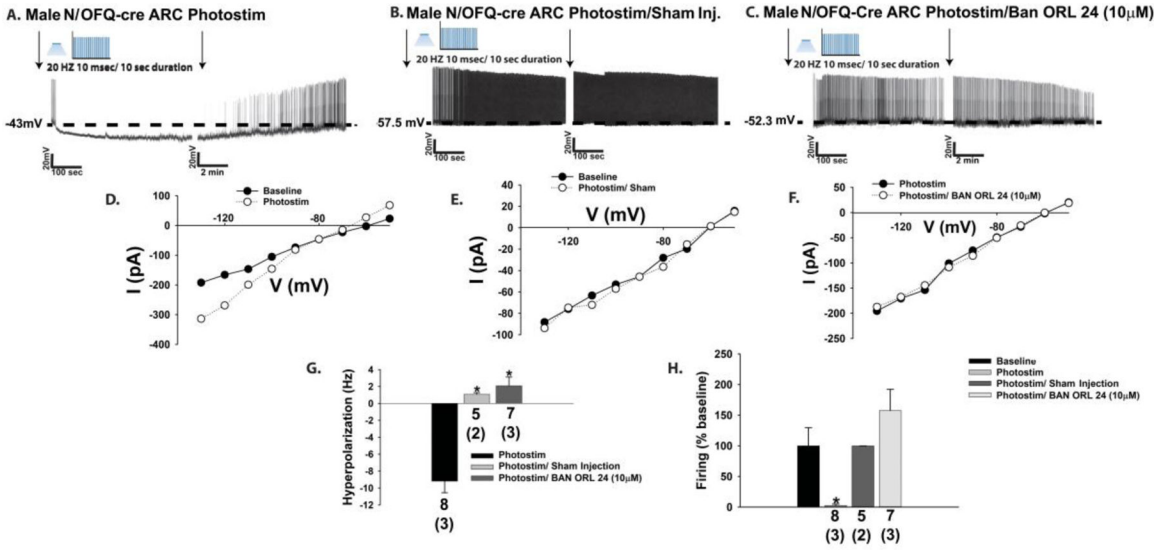

Fig. 2.

The photostimulation (photostim)-induced outward current in POMC neurons is associated with a hyperpolarization and a decrease in firing, which is abrogated by BAN ORL 24. **(A**; n=8) Representative trace of a current clamp recording in a slice from an intact male N/OFQ-cre/eGFP-POMC mouse showing the reversible hyperpolarization and decrease in firing (n = 8) that is not apparent in slices pre-treated with BAN ORL 24 **(C**; n=7) or injected (inj.) with an eYFP blank-containing AAV **(B**; n=5). **D-F**, the photo-stimulation-induced increase in slope conductance (or lack thereof) faithfully mirrors the extent of the hyperpolarization and decrease in firing. These effects are summarized in the composite bar graphs seen in **G** and **H**. Bars represent means, and lines 1 SEM of the hyperpolarization magnitude (mV; **G**) and the change in firing (**H**). Numbers above parenthesis in bar graphs are indicative of the number of cells recorded for that treatment, while numbers in parenthesis are indicative of the number of animals used for that treatment. *$p < 0.05$, relative to photostimulation alone, one-way ANOVA/LSD (**G**); relative to baseline, Kruskal-Wallis/median-notched box-and-whisker analysis (**H**).

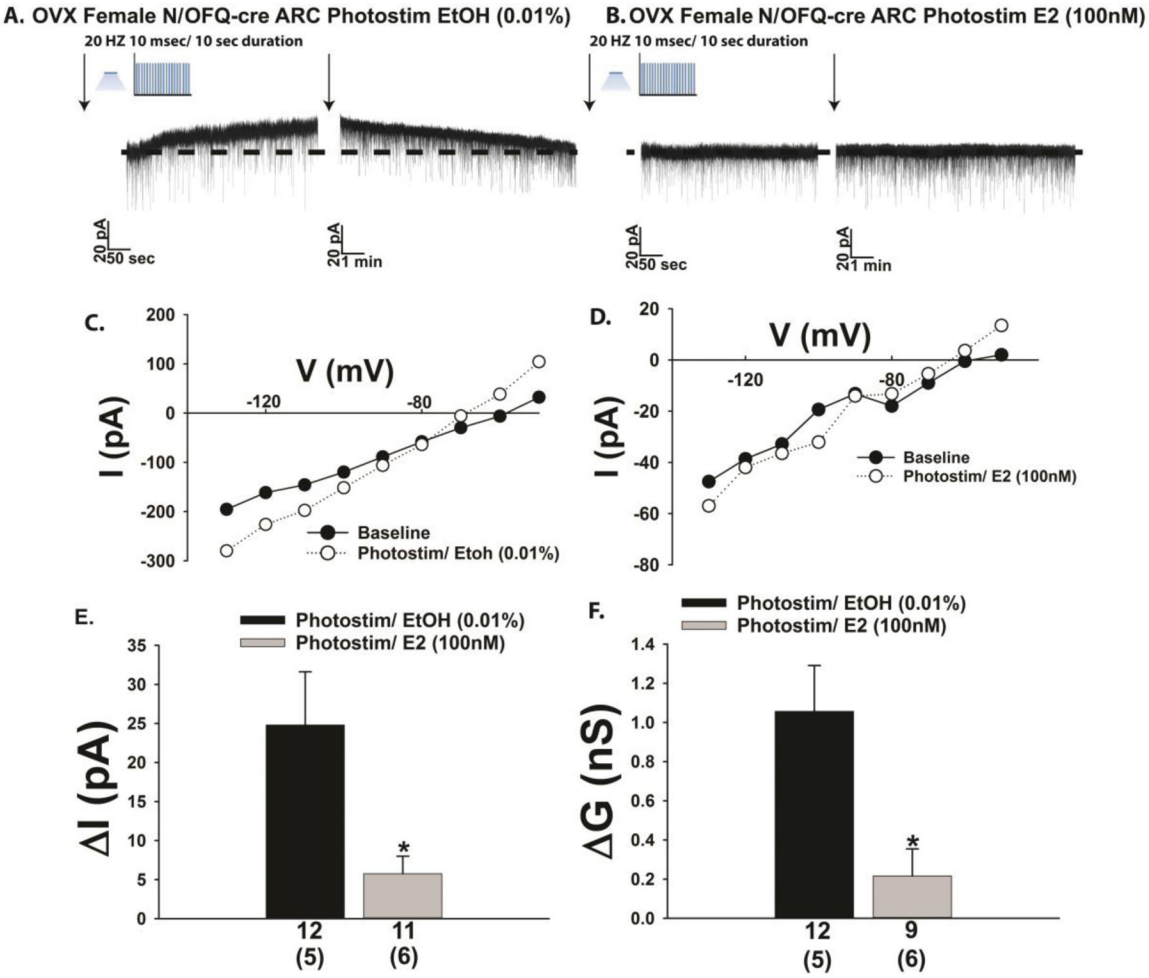

Fig. 3.

Optogenetic stimulation of ARC N/OFQ neurons produces an outward current in POMC neurons from OVX female N/OFQ-cre/eGFP-POMC mice, which is markedly attenuated by E_2. **(A)** Membrane current trace showing the robust and reversible outward current (n = 12) during a recording from an ethanol (EtOH; 0.01% v:v) vehicle pre-treated slice. The magnitude of this current is dramatically dampened by E_2 (100 nM; **B**; n = 11). **C & D**, Parallel changes were observed with the photostimulation (photostim)-induced increase in slope conductance. These effects are captured in composite form in **E** and **F**. Bars represent means, and lines 1 SEM of the change in membrane current (pA; **E**) and conductance (nS; **F**). Numbers above parenthesis in bar graphs are indicative of the number of cells recorded for that treatment, while numbers in parenthesis are indicative of the number of animals used for that treatment. *$p < 0.05$, relative to EtOH vehicle alone, Student's t-test.

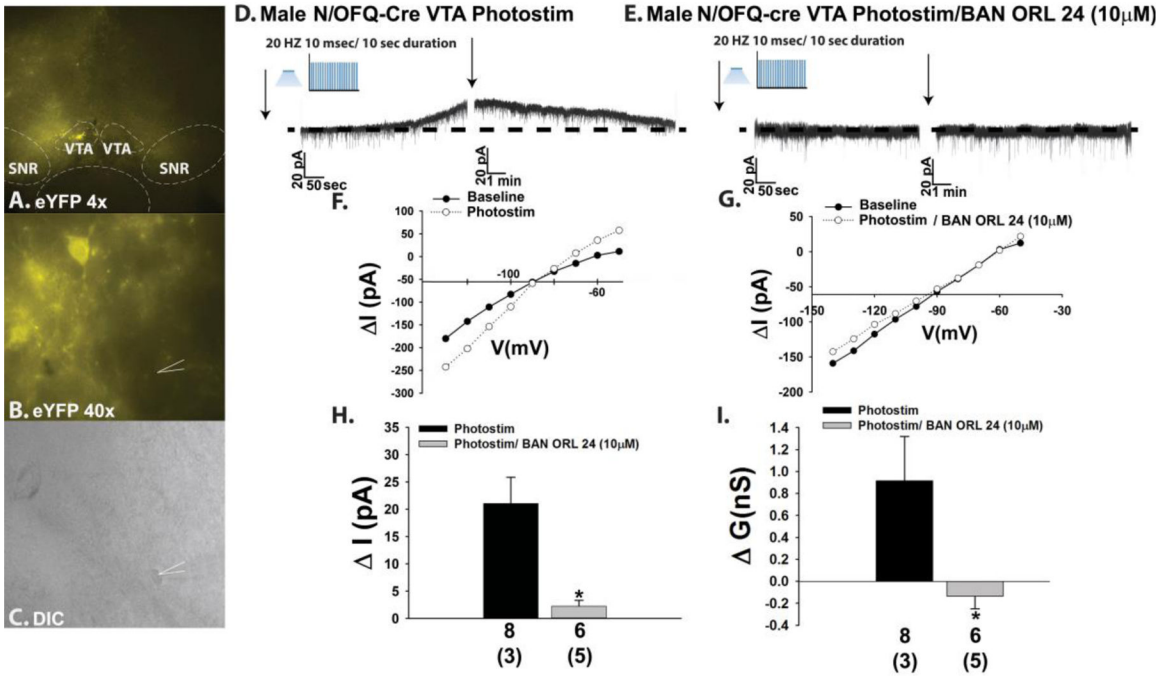

Fig. 4.

Optogenetic activation of VTA N/OFQ neurons in male mice induces NOP receptor-mediated outward currents in downstream neurons receiving synaptic input. **A** & **B**, eYFP ChR2 reporter staining in the VTA at 4X and 40X. **C**, DIC image of a recorded neuron surrounded by the eYFP-filled N/OFQ fibers seen in **B**. **D**-**G**, Photostimulation (photostim) of N/OFQ neurons elicits a reversible outward current in the cell in **C** due to activation of a K^+ conductance via a NOP receptor-mediated mechanism (**D**: n = 8; **E**: n = 6). These effects are compositely expressed in **H** and **I**. Bars represent means, and lines 1 SEM of the change in membrane current (ΔI; **H**) and slope conductance (Δg; **I**). Numbers above parenthesis in bar graphs are indicative of the number of cells recorded for that treatment, while numbers in parenthesis are indicative of the number of animals used for that treatment. *$p < 0.05$, relative to photostimulation alone, Student's t-test.

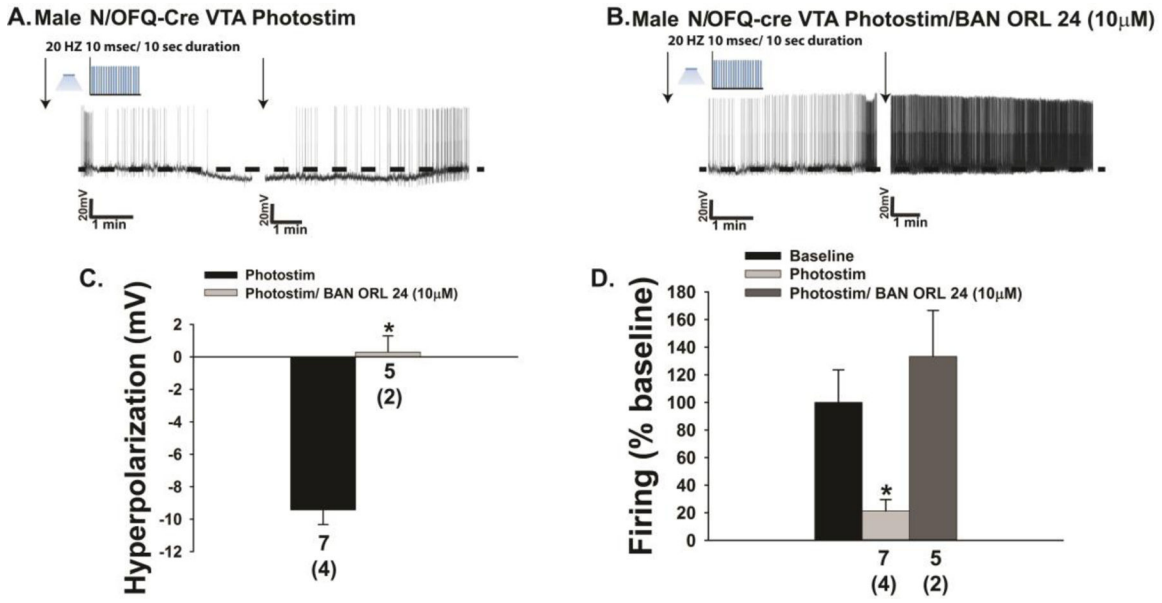

Fig. 5.

The outward current caused by photostimulation (photostim) of VTA N/OFQ neurons corresponds with a NOP receptor-mediated membrane hyperpolarization and reduction in firing. **A & B**, Representative voltage traces depicting the photostimulation-induced hyperpolarization (n = 7) and abolition of firing that are antagonized by BAN ORL 24 (n = 5). The composite bar graphs in **C** and **D** summarize these effects. Bars represent means, and lines 1 SEM of the change in membrane voltage (**C**; mV) and the change in firing relative to baseline (**D**). Numbers above parenthesis in bar graphs are indicative of the number of cells recorded for that treatment, while numbers in parenthesis are indicative of the number of animals used for that treatment. *$p < 0.05$, relative to photostimulation alone, Student's t test (**C**); Kruskal-Wallis/median-notched box-and-whisker analysis (**D**).

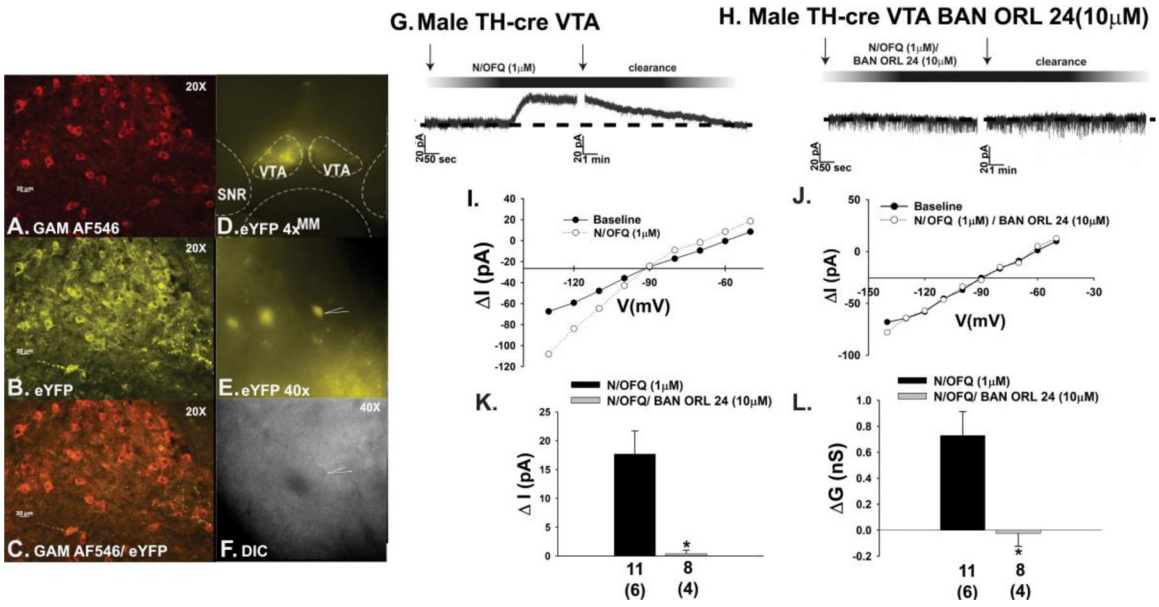

Fig. 6.

N/OFQ elicits an outward current in A_{10} dopamine neurons during voltage clamp recordings in slices from male TH-cre mice via a NOP receptor-mediated mechanism. **A**, TH immunostaining in the VTA. **B**, eYFP signal seen in these A_{10} dopamine neurons. **C**, composite overlay. **D** & **E**, eYFP signal from A_{10} dopamine neurons in VTA slices seen at 4X and 40X. **F**, DIC image of the recorded A_{10} dopamine neuron seen in **E**. **G** & **H**, Bath applied N/OFQ (1 μM) produces a robust and reversible outward current in A_{10} dopamine neurons (n = 11) that is abrogated by BAN ORL 24 (n = 8). **I & J**, This NOP receptor-mediated response is associated with an increased K^+ conductance. These effects are summarized compositely in **K** and **L**. Bars represent means and lines 1 SEM of the change in membrane current (**K**; pA) and slope conductance (**L**; nS). Numbers above parenthesis in bar graphs are indicative of the number of cells recorded for that treatment, while numbers in parenthesis are indicative of the number of animals used for that treatment. *$p < 0.05$ relative to N/OFQ alone, Student's t-test.

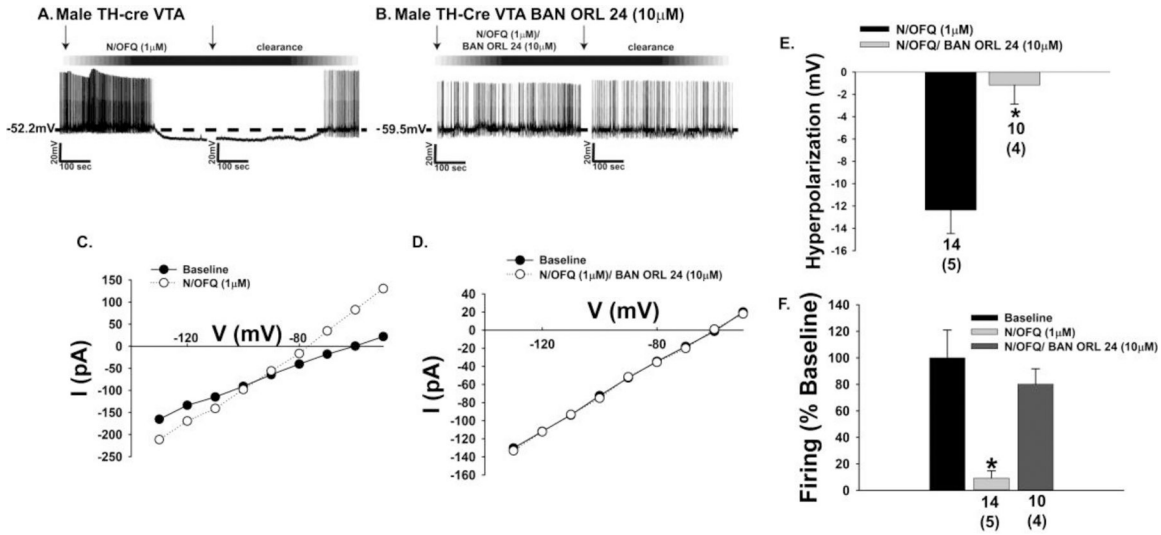

Fig. 7.

The NOP receptor-mediated outward current in A_{10} dopamine neurons in male mice is associated with a membrane hyperpolarization and cessation of firing. **A & B**, Representative voltage traces obtained during current clamp recordings in slices from male TH-cre mice illustrating the N/OFQ-induced hyperpolarization (n = 14) and suppression of firing that is negated by BAN ORL 24 (n = 10). **C & D**, These effects are mirrored by the increase in K^+ conductance or lack thereof, and summarized compositely in **E** and **F**. Bars represent means and lines 1 SEM of the hyperpolarization (**E**; mV) and change in firing relative to baseline (**F**). Numbers above parenthesis in bar graphs are indicative of the number of cells recorded for that treatment, while numbers in parenthesis are indicative of the number of animals used for that treatment. *$p < 0.05$, relative to photostimulation alone, Student's t test (**E**); Kruskal-Wallis/median-notched box-and-whisker analysis (**F**).

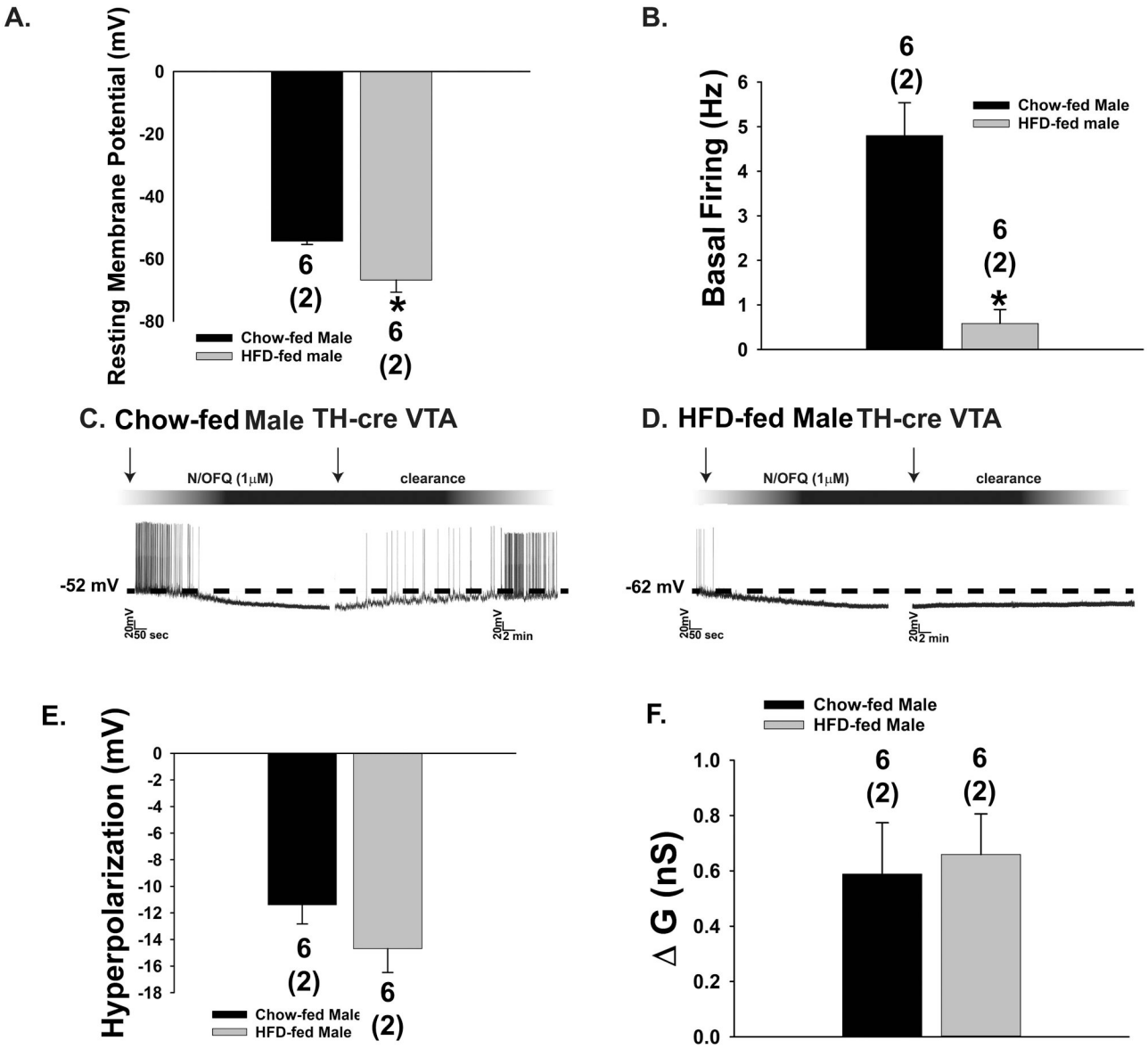

Fig. 8.

Diet-induced obesity renders A_{10} dopamine neurons more quiescent and prolongs the inhibitory effect of N/OFQ. Composite bar graphs depicting the markedly hyperpolarized RMP (**A**) and reduced basal firing rate (**B**) seen in A_{10} dopamine neurons from obese TH-cre males. **C & D**, Representative voltage traces from chow-(n = 22) and HFD-fed (n = 12) males illustrating the more prolonged inhibitory response of A_{10} dopamine neurons to N/OFQ under conditions of diet-induced obesity. The last two bar graphs show the lack of effect of diet-induced obesity on the magnitude of the N/OFQ-induced hyperpolarization (**E**) or change in conductance (**F**). Bars represent means and line 1 SEM. Numbers above parenthesis in bar graphs are indicative of the number of cells recorded for that treatment, while numbers in parenthesis are indicative of the number of animals used for that treatment. *$p < 0.05$, relative to chow-fed controls, Student's t-test.

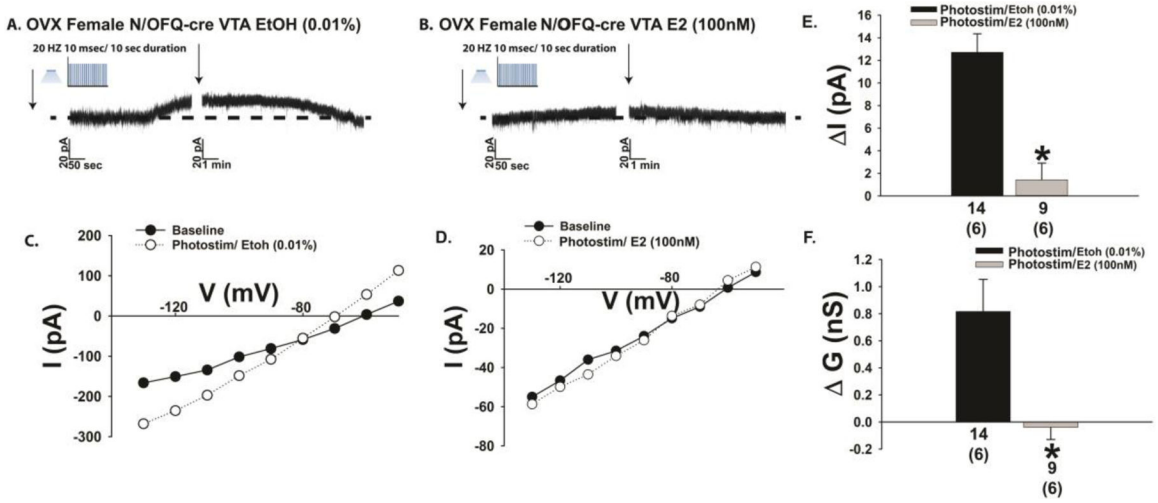

Fig. 9.

E_2 attenuates the outward current caused by optogenetic stimulation of VTA N/OFQ neurons during voltage clamp recordings in slices from OVX female N/OFQ-cre mice. **A & B**, Representative traces show the estrogenic diminution in the magnitude of the photostimulation (photostim)-induced outward current (**A**: n = 14; **B**: n = 9) as well as the accompanying increase in slope conductance shown in **C** and **D**. These effects are compositely represented in the bar graphs shown in **E** and **F**. Bars represent means and lines 1 SEM of the change in membrane current current (**E**; pA) and slope conductance (**F**; nS). Numbers above parenthesis in bar graphs are indicative of the number of cells recorded for that treatment, while numbers in parenthesis are indicative of the number of animals used for that treatment. *$p < 0.05$ relative to EtOH vehicle, Student's t-test.

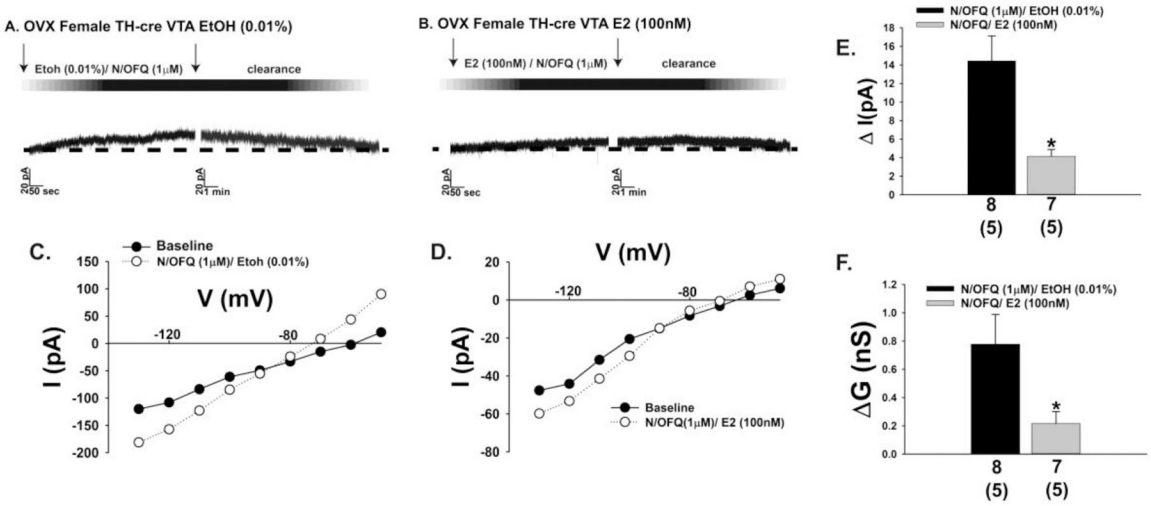

Fig. 10.

E_2 diminishes the outward current in A_{10} dopamine neurons caused by exogenously administered N/OFQ during voltage clamp recordings in slices from OVX female TH-cre mice. **A & B**, Representative traces illustrating how E_2 reduces the amplitude of the outward current caused by bath application of N/OFQ (**A**: n = 8; **B**: n = 7) along with the increase in slope conductance shown in **C** and **D**. These effects are compositely expressed in the bar graphs shown in **E** and **F**. Bars represent means and lines 1 SEM of the change in membrane current current (**E**; pA) and slope conductance (**F**; nS). Numbers above parenthesis in bar graphs are indicative of the number of cells recorded for that treatment, while numbers in parenthesis are indicative of the number of animals used for that treatment. *$p < 0.05$ relative to EtOH vehicle, Student's t-test (E).

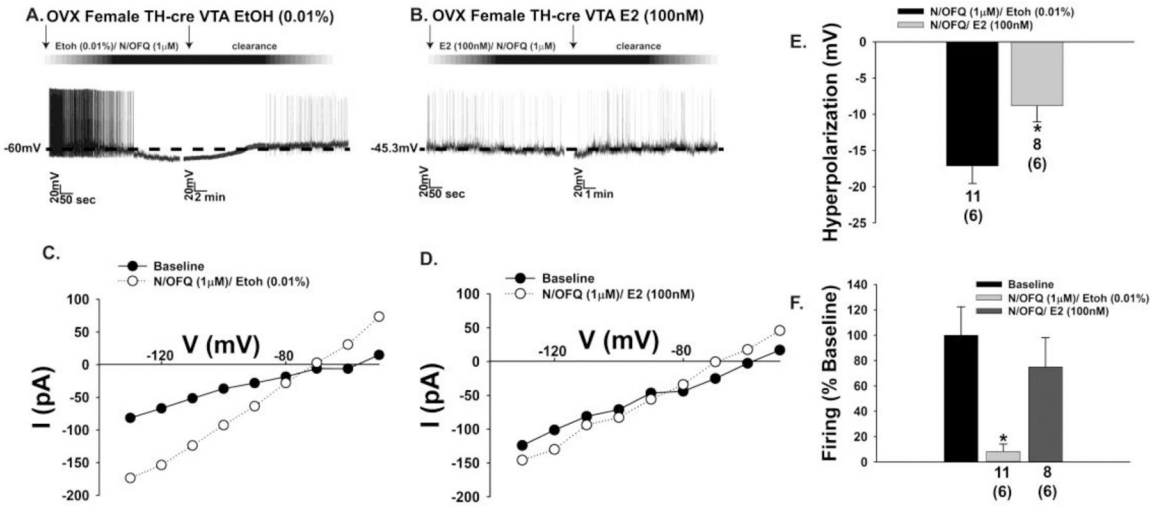

Fig. 11.

Likewise, E_2 dampens the N/OFQ-induced membrane hyperpolarization and abolition of firing seen in A_{10} dopamine neurons during current clamp recordings in slices from OVX female TH-cre mice. **A & B**, Representative traces depicting how E2 physiologically antagonizes the hyperpolarization and decrease in firing caused by N/OFQ (**A**: n = 11; **B**: n = 8), as well as the increase in K^+ conductance shown in **C** and **D**. These changes are reflected in the composite bar graphs of **E** and **F**. Bars represent means and lines 1 SEM of the hyperpolarization (**E**; mV) and change in firing relative to baseline (**F**). Numbers above parenthesis in bar graphs are indicative of the number of cells recorded for that treatment, while numbers in parenthesis are indicative of the number of animals used for that treatment. *$p < 0.05$, relative to EtOH alone, Student's t test (**E**); Kruskal-Wallis/median-notched box-and-whisker analysis (**F**).

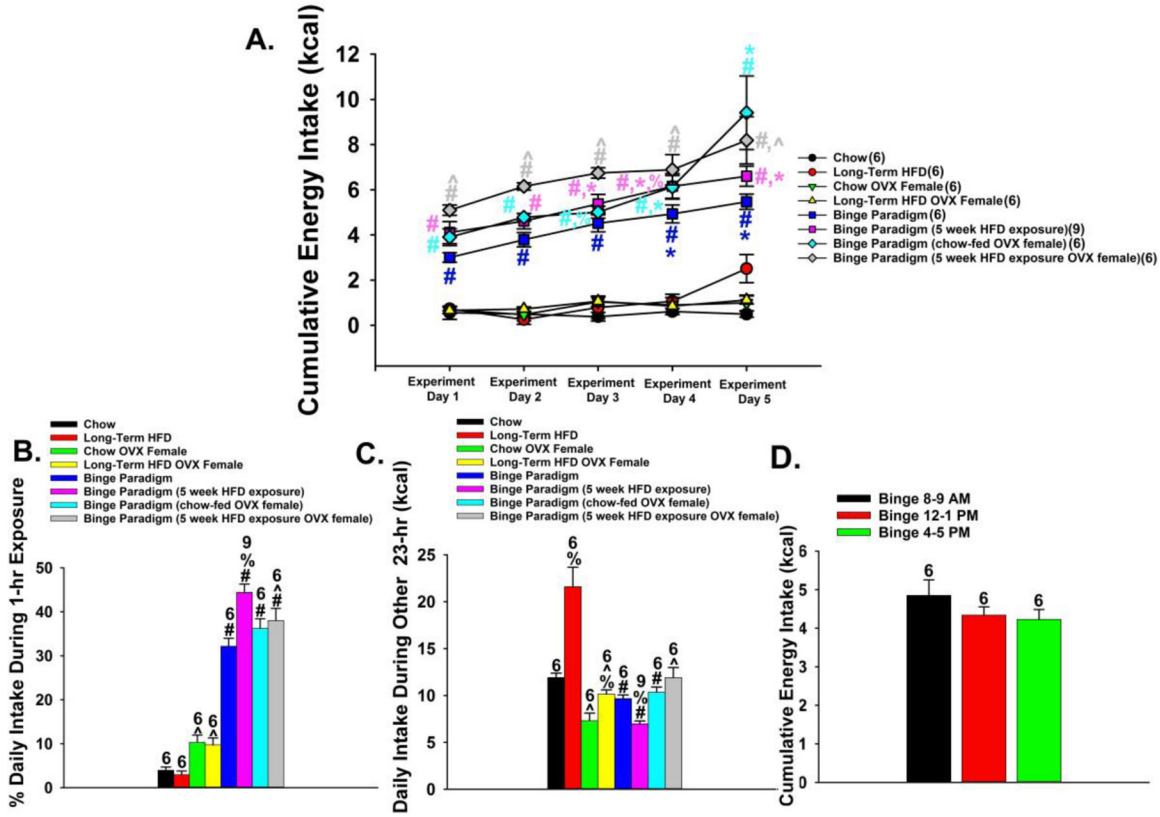

Fig. 12.

Intermittent access to HFD dramatically escalates consumption in wildtype mice, which is accentuated by diet-induced obesity and hypoestrogenic conditions. **A**, Time course illustrating the rapidity of the escalation in binge eating over the five days of the monitoring period, which is especially prominent in obese males and OVX females. **B**, Bar graph illustrating the disproportionate energy consumption during the one-hour exposure to HFD; particularly in obese males. **C**, Bar graph depicting cumulative energy intake observed during the other 23 hours of the day. D, Bar graph demonstrating that the extensive binge-like hyperphagia occurs irrespective of time of day. Bars represent means and vertical lines 1 SEM. Numbers above bars indicate number of animals used per treatment group. *, $p < .05$ relative to binge day 1; #, $p < .05$ relative to non-binging controls; ^, $p < .05$ relative to males; %, $p < .05$ relative to chow-fed controls, repeated measures multi-factorial ANOVA/ LSD, $n = 6 – 9$.

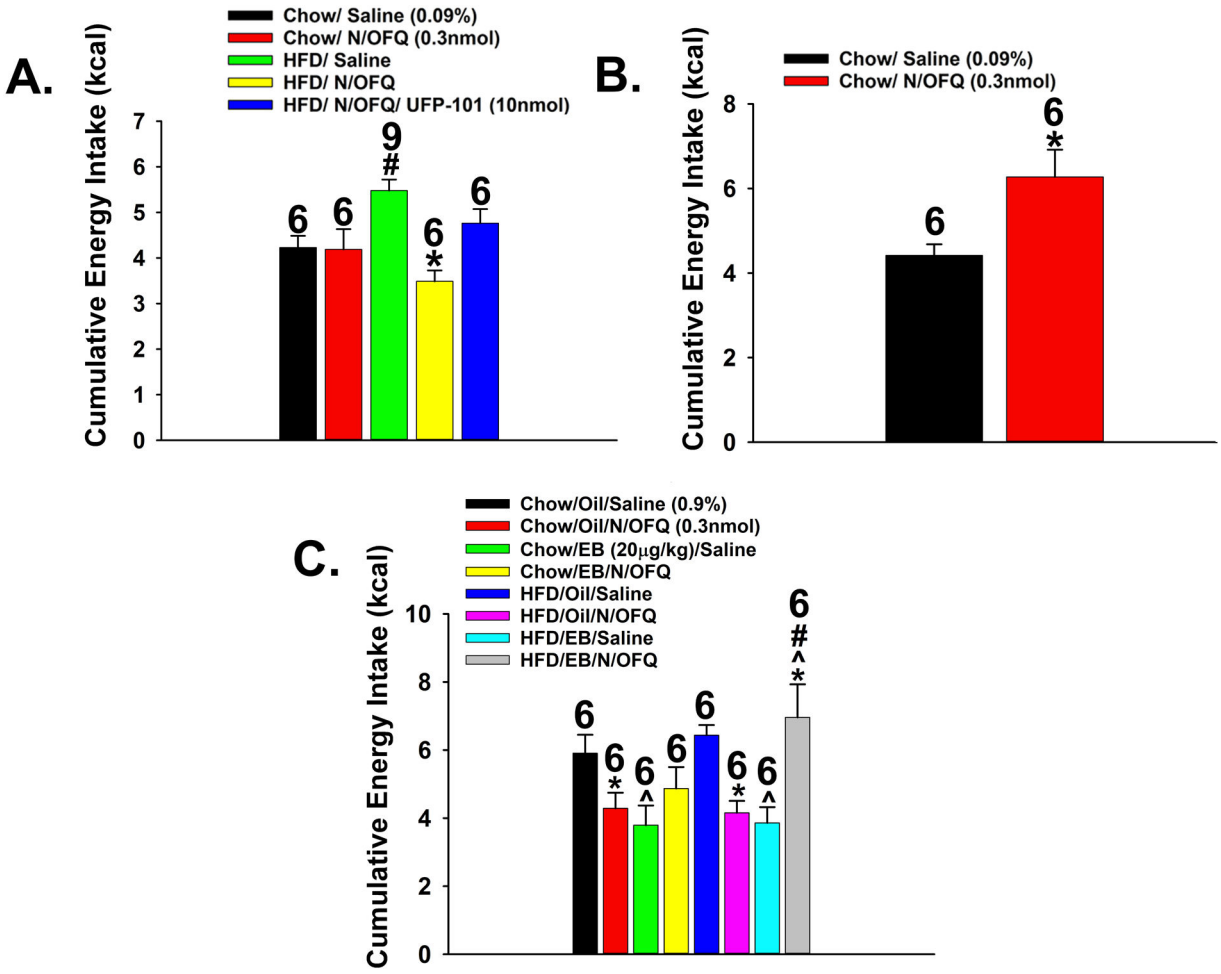

Fig. 13.

NOP receptors regulate binge-eating behavior in a site- and sex-specific manner. **A**, Bar graph depicting how intra-VTA N/OFQ (0.3 nmole/0.2 μL) dampens the escalation in the consumption of palatable food seen in males exposed to HFD for five weeks prior to commencing the binge-feeding protocol; an effect attenuated by the NOP receptor antagonist UFP-101 (10 nmole/0.2 μL). **B**, Bar graph illustrating that intra-ARC N/OFQ potentiates binge feeding in male mice. **C**, Bar graph demonstrating that the N/OFQ-induced decrease in the binge-like intake seen in sesame oil-treated (1 mL/kg; s.c.) OVX female mice is reversed by EB treatment (20 μg.kg; s.c.); particularly in those rendered obese following five weeks of HFD feeding. Numbers above bars indicate number of animals used per treatment group. *, $p < .05$ relative to saline-treated controls; #, $p < .05$ relative to lean controls; ^, $p < .05$ relative to sesame oil-treated controls, repeated measures multi-factorial ANOVA/LSD, n = 6 – 9.